Technical Report No. 32-644

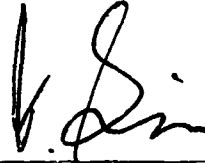# Errors Associated With Spinning-Up and Thrusting Symmetric Rigid Bodies

R. S. Armstrong

jpl JET PROPULSION LABORATORY
CALIFORNIA INSTITUTE OF TECHNOLOGY
PASADENA, CALIFORNIA

February 15, 1965

Technical Report No. 32-644

Errors Associated With Spinning-Up and Thrusting Symmetric Rigid Bodies

R. S. Armstrong

W. Gin, Chief
Solid Propellant Engineering Section

CONTENTS

CONTENTS (Cont'd)

TABLES

FIGURES

FIGURES (Cont'd)

FIGURES (Cont'd)

ABSTRACT

/7 865

The equations defining errors generated during the spin-up of symmetric rigid bodies and subsequent thrusting of the spinning body are derived from Euler's dynamical equations and transformed into inertial coordinates. Examples of both spin-up and thrusting errors are given for the *Ranger* lunar landing capsule and an Apollo-shaped planetary entry capsule.

The stability of nonrigid spinning symmetrical bodies is also discussed. Equations describing the precessional motion are given, and a simple mathematical model is analyzed. Results indicate that to minimize errors in the spin-up and thrusting phase, a high spin-rate is desired, whereas to minimize errors during coast, a low spin-rate is needed.

I. INTRODUCTION

More than a dozen space projects have successfully utilized spin stability as a mode of attitude control; many other space applications have been viewed analytically. This Report deals with three phases of spin stability—the spin-up process itself, thrusting the rigid body after spin-up, and the stability of not-so-rigid bodies during coast.

Two projects presently under the auspices of the Jet Propulsion Laboratory (JPL) have investigated this area. They are the *Ranger* Blocks II and V and the *Mariner* Mars '66. The *Ranger* rough-landing capsule was to have been separated from the parent spacecraft by spinning-up with canted nozzles (to a nominal 350 rpm in 1 sec), so that a positive separation velocity was attained during spin-up. Shortly after separation, a solid propellant rocket motor (which constituted roughly ⅔ of the total

mass) was ignited, removing approximately 8800 ft/sec from the incoming velocity vector. It was necessary to determine the velocity vector at motor burnout.

The possibility of a planetary entry capsule to be separated from the fly-by spacecraft was considered for the *Mariner* Mars '66 mission, and is definitely being considered for future planetary missions. The physical separation of the capsule from the spacecraft, and the accuracy of the required velocity vector were studied. One method involved releasing the capsule from the bus with springs, spinning-up immediately, coasting for a while (to ensure minimal impingement of the rocket exhaust on the spacecraft), then igniting a rocket motor to give the required separation velocity. For most velocities considered, a constant capsule mass (during burning) could be assumed. The question arose as to how accurate

the velocity vector was when added to the capsule, considering the spin-up as well as the thrusting errors. Another question which arose was with regard to the stability of the capsule after the entire separation maneuver (if it were still spinning at its design rate). If stability was required (say, for telecommunications), then a recurrence of what happened on *Explorer I*[1] could not be tolerated.

It is believed that the tools necessary for the solution of the three aforementioned problems, and sufficient

---

[1]Shortly after launch, *Explorer I*, a satellite shaped like a cigar and spun about its axis of symmetry, began to increase its wobble angle until finally all spin was about the transverse axis.

examples, are given so that the conclusion and equations may be generally applied.

In the spin-up and thrusting Sections (III and IV), the applied torques are assumed body-fixed and constant. Neither gravity nor solar pressure affects the errors since they are inertial forces. Aerodynamic forces are not considered.

Since the areas discussed in Sections III, IV and V were investigated separately, each Section is self contained, and depends at most on the general discussion in Section II.

II. RIGID BODY EQUATIONS OF MOTION

A. Euler's Dynamical Equations

Consider the rotational analog of Newton's second law of motion in inertial coordinates:

$$L = \frac{d}{dt}(J) = \frac{d}{dt}(\Pi\,\Omega) \qquad (1)$$

where L is the external torque, J the angular momentum, Π the inertia tensor[2], and Ω the angular velocity. Recalling that the time rate of change of a vector (A) in a moving reference frame of angular velocity (Ω) with respect to some inertial frame is $[\dot{A}]_{\text{inertial}} = [\dot{A}]_{\text{body-fixed}} + [\Omega \times A]$, Eq. (1) may be rewritten

$$L = \left[\frac{d}{dt}(\Pi\,\Omega)\right]_{\text{inertial}} = \left[\frac{d}{dt}(\Pi\,\Omega)\right]_{\text{body-fixed}} + \Omega \times (\Pi\,\Omega) \qquad (2)$$

The Ω in the above equations is that of the moving frame with respect to the inertial frame. The torque (L) has been constrained to be body-fixed.

Equation (2), when expanded, yields[3];

$$I_x\,\dot{\omega}_x - (I_y - I_z)\,\omega_y\,\omega_z = L_x \qquad (3a)$$

$$I_y\,\dot{\omega}_y - (I_z - I_x)\,\omega_x\,\omega_z = L_y \qquad (3b)$$

$$I_z\,\dot{\omega}_z - (I_x - I_y)\,\omega_x\,\omega_y = L_z \qquad (3c)$$

Equations (3) are Euler's dynamical equations, the basic tool for the analysis carried out in this Report.

If the z-axis is taken to be the axis of symmetry and of spin[4] (whereupon $I_x = I_y$), then a convenient method of presenting the cross-angular velocities is obtained by

---

[2]For the results discussed in this Report, Π is diagonal, i.e., the cross products of inertia are zero. When a body of symmetry is designed to be spun, dynamic balancing can move the principal axes of rotation coincident with the geometrical axes to a degree beyond that of interest to this study. However, for the case where the products of inertia cannot be assumed zero, and for the effects of products of inertia on spin-up, an excellent treatment is given in Ref. 1.

[3]The rate of change of inertia component in $\frac{d}{dt}(\Pi\,\Omega)$, i.e., $\dot{I}_x\omega_x$, etc., must be assumed zero, since $\dot{I}_x$, etc., must necessarily be caused by a mass expenditure which is no longer part of the rigid body. If not, and $\dot{I}_x$, etc., is not the result of a dm/dt, then the assumption of a rigid body is no longer valid.

[4]Spin is defined as the rotation about the body roll axis (ω_z) only, and the cross plane rotation $(\omega_x$ and $\omega_y)$ is referred to as wobble.

letting $\omega = \omega_x + i\,\omega_y$, thereby mapping both components onto the complex plane. Noting that $\dot{\omega} = \dot{\omega}_x + i\,\dot{\omega}_y$, Eqs. (3a and 3b) combine to give

$$\dot{\omega} - i\,\lambda\,\omega\,\omega_z = N \qquad (4)$$

where $\lambda = I_z/I_x - 1$, $(-1 < \lambda < 1)$, and $N = \dfrac{L_x + iL_y}{I_x}$ (cross-angular acceleration). Since $I_x = I_y$, Eq. (3c) reduces to

$$\dot{\omega}_z = \frac{L_z}{I_z} = N_z \quad \text{(angular acceleration of spin)} \qquad (5)$$

It will be shown later that N_z must be a constant for any reasonable closed form of Eq. (4) and subsequent equations.

If all torques are zero on the body, then $\omega_z = \text{constant} = s_0$ (initial spin rate), whereupon Eq. (4) is immediately integrated to

$$\omega = \omega_0\,\epsilon^{i\lambda s_0 t} \qquad (6)$$

where $\omega_0 = \omega_{0x} + i\,\omega_{0y}$. The components of Eq. (6) are

$$\omega_x = \mathcal{R}_e\,\omega = \omega_{0x}\cos\lambda\,s_0\,t - \omega_{0y}\sin\lambda\,s_0\,t$$

$$\omega_y = \mathcal{I}_m\,\omega = \omega_{0y}\cos\lambda\,s_0\,t + \omega_{0x}\sin\lambda\,s_0\,t$$

When time is eliminated as a parameter, it is seen that the magnitude of the cross-angular velocity is constant, $\omega = (\omega_{0x}^2 + \omega_{0y}^2)^{1/2}$, and rotating about the angular momentum vector J at a frequency $\lambda\,s_0$.

Note that the magnitude of the spin rate, ω_z, is dependent on s_0 and N_z alone, hence would remain constant regardless of the value of $N = N_x + i\,N_y$. This is true only because the body is symmetrical.

B. Inertial Transformation

The transformation from body-fixed coordinates to inertial coordinates is made with conventional Euler angles.[5] The $X_0 - Y_0 - Z_0$ frame is inertial, the $x - y - z$ frame being body-fixed. The three angular rotations are

---

[5]Another Eulerian angular transformation for analog computer simulation is given in Appendix A.
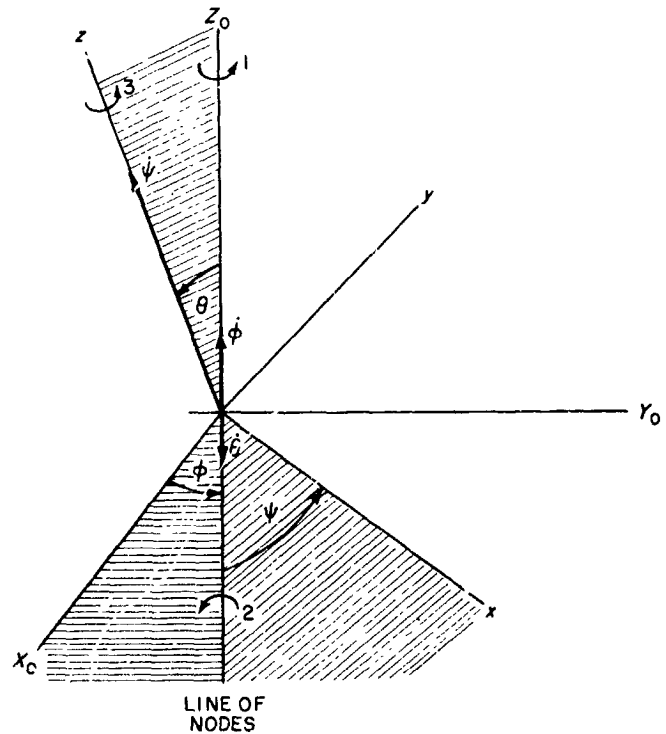
Fig. 1. Euler angle transformation

shown in order on Fig. 1, and are discussed more fully in Ref. 2. They are

$$[\phi] = \begin{bmatrix} \cos\phi & \sin\phi & 0 \\ -\sin\phi & \cos\phi & 0 \\ 0 & 0 & 1 \end{bmatrix};$$

$$[\theta] = \begin{bmatrix} 1 & 0 & 0 \\ 0 & \cos\theta & \sin\theta \\ 0 & -\sin\theta & \cos\theta \end{bmatrix};$$

$$[\psi] = \begin{bmatrix} \cos\psi & \sin\psi & 0 \\ -\sin\psi & \cos\psi & 0 \\ 0 & 0 & 1 \end{bmatrix} \qquad (7)$$

As seen in Fig. 1, the transformation from Euler rates to body-fixed rates is

$$\begin{bmatrix} \omega_x \\ \omega_y \\ \omega_z \end{bmatrix} = \begin{bmatrix} \sin\theta\,\sin\psi & \cos\psi & 0 \\ \sin\theta\,\cos\psi & -\sin\psi & 0 \\ \cos\theta & 0 & 1 \end{bmatrix} \begin{bmatrix} \dot{\phi} \\ \dot{\theta} \\ \dot{\psi} \end{bmatrix} \qquad (8)$$

The full angular transformation $[\psi] \cdot [\theta] \cdot [\phi]$ is discussed in Section IV-E.

If the cross-angular velocities $(\omega_r + i \omega_y)$ are mapped onto the complex plane from Eq. (8),

$$\omega = (\dot{\theta} + i \dot{\phi} \sin \theta) e^{-i\psi} \qquad (8a)$$

which becomes (when $\dot{\phi}$ is eliminated):

$$\omega = [\dot{\theta} + i (\omega_z - \dot{\psi}) \tan \theta] e^{-i\psi}$$

If a small angle approximation for θ is made, which is valid in light of the small errors to be encountered, then $(\theta \approx \tan \theta)$

$$\omega = [\dot{\theta} + i (\omega_z - \dot{\psi}) \theta] e^{-i\psi}$$

Defining a complex angle of attack by

$$a = \theta e^{-i\psi}$$

then ω and a are related by

$$\dot{a} + i \omega_z a = \omega \qquad (9)$$

which can be verified by substitution. This complex angle of attack $a = \theta (\cos \psi - i \sin \psi)$ is seen from Fig. 1 to be the angle of attack (θ) as seen by an observer sitting on the X_0-axis for $\mathcal{R}_e$ a and the $-Y_0$ axis for $\mathcal{I}_m$ a. How-

ever, a is only a mathematical intermediary to obtain the inertial angle of attack in complex form. This is given by

$$a_I = a \, e^{i \int \omega_z dt} \qquad (10)$$

This can be shown as follows: From Eq. (8), $\omega_z = \dot{\phi} \cos \theta + \dot{\psi}$ and $\cos \theta \approx 1$,

$$i \int \omega_z \, dt = i \int (\dot{\phi} \cos \theta + \dot{\psi}) \, dt = i \int (\cos \theta \, d\phi + d\psi)$$
$$= i (\phi + \psi)$$

whence Eq. (10) becomes

$$a_I = a \, e^{i(\phi+\psi)} = \theta e^{-i\psi} e^{i(\phi+\psi)} = \theta e^{i\phi} \qquad (11)$$

Equation (11) then is the full inertial transformation, for expanding $a_I = \theta (\cos \phi + i \sin \phi)$, which is the angle of attack θ as seen by an observer sitting on the X_0-axis when $\phi = 0$, and the Y_0-axis when $\phi = \pi/2$. Thus, $\mathcal{R}_e$ a_I will give the X_0-component of the time-varying angle of attack, and $\mathcal{I}_m$ a_I, the Y_0-component.

In a similar manner, it can be shown that the complex angular rate as measured in the inertial $X_0 - Y_0$ direction is

$$\omega_I = \omega \, e^{i \int \omega_z dt}$$

III. SPINNING-UP OF SYMMETRIC RIGID BODIES

When a symmetric rigid body is free in space with an initial rotation $(\dot{\theta}_0)$ about its pitch-yaw axis, and is then torqued about its roll axis to a spinning condition, three errors result:

1. The angular displacement at the moment of spin-up due to the initial conditions Θ_0 and $\dot{\theta}_0$. That is, with respect to the inertial reference, there is an angular displacement error (Θ_0), a rate error $(\dot{\theta}_0)$, and a time from release to spin-up (δt) which causes an angle of $\Theta_0 + \dot{\theta}_0 \delta t$ between the body-fixed z-axis and the true inertial axes at the time between release and spin-up of the body. Since Θ_0 and δt are parameters which are totally independent of this analysis, their effect is omitted here, but must be

determined and vectorially summed with the errors listed below for a full separation error analysis.[6] The new inertial axes are then defined as the body-fixed axes at $t = 0$, thus omitting this angular error from further consideration.

2. When the body is spun-up about the new set of inertial axes, it is found that the angular momentum vector, which defines the direction of spin, is displaced at an angle a_I. This rotation of J is the result of both the initial tumble rate $(\dot{\theta}_0)$ and the errors associated with the spin-up itself, which arise out of the body trying to spin-up about axes other

---

[6]See section III-D.

than principal, thus generating cross products of inertia.

3. The body-fixed z-(spin) axis rotates about the angular momentum vector at an angle β. This wobble is caused also by both initial and spin-up errors. In the analysis, β is derived first since the development of a_t depends on β.

A. Spin Jet Misalignment

The errors in the spin-up are caused by an initial condition and an error associated with the alignment of the body-fixed torque vector. This error in the torque vector is made up of the five components shown in Fig. 2. If there are n spin jets, the nominal thrust of each being F, and if the jets are evenly spaced about a circle of radius R, the plane of which is i from the c.m. of the body, the torque in the z-direction is (using small angle approximations)

$$L_z = n F R \qquad (12)$$

The possible effects of ΔR on L_z are neglected. By inspection of Fig. 2, the RSS cross-plane (i.e., x-y) torques are[7]

$$L = \left\{ nF^2 \left[(R\xi)^2 + (\Delta l)^2 + (\eta l)^2 \right] + n (l\Delta F)^2 \right\}^{1/2} \qquad (13)$$

If $\Delta F = kF$, which is the case when spin jets are manifolded $L = \sqrt{n}\, F\, (a + ib)$, the complex number being for the direction of the net cross-plane torque which is not known from Eq. (13). However, when the cross-plane torque is compared to the primary torque, it is seen that

$$L = L_x + i L_y = \gamma L_z \qquad (14)$$

---

[7]Assuming the misalignments are randomly distributed and no biases exist, especially in alignment tooling. If biases do exist, then Eq. (13) is conservative.

(a) (b)
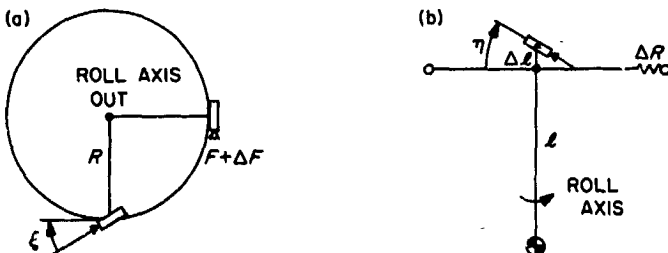
Fig. 2. Spin jet misalignments: a. top view; b. side view

where

$$\gamma = \frac{a + i\, b}{\sqrt{n}\, R}$$

Equation (14) is the form which will be used for the cross-plane torque. γ is defined as a real number without loss in generality. Furthermore, the body-fixed x-y axes and the inertial X_0-Y_0 axes are defined to make the initial rate $\dot{\theta}_0$ and the cross-plane torque L act in the same direction, thus presenting a worst case.

B. Primary Torque Considerations

The cross-plane angular acceleration is

$$N = \frac{L}{I_x} = \frac{\gamma L_z}{I_x} = \frac{I_z}{I_x} \gamma N_z = (1 + \lambda) \gamma N_z \qquad (15)$$

Eliminating ω_z from Eqs. (4) and (5),

$$\omega - i \lambda \omega \int N_z \, dt = \gamma (1 + \lambda) N_z \qquad (16)$$

It is immediately seen that the form of N_z governs the solubility of Eq. (16)[8]. In general, the $\int N_z \, dt$ introduces a constant of integration, the initial spin rate ω_{0z}. If partial restraint of the body during spin-up is made, $\omega_{0z} > 0$, and Eq. (16) has no analytic solution. Therefore, $\omega_{0z} = 0$ from here on.

Even after making $\omega_{0z} = 0$, the form of N_z is quite restricted for closed solutions. If a cold gas spin-up system is considered, then $\int N_z \, dt = c(1 - e^{-rt})$, since an exponential decay of thrust (and an exponential increase in spin rate) is the best approximation. As can be verified by substitution, the constant value c acts in the same way that ω_{0z} does in the solubility of Eq. (16), preventing a closed form solution. Polynomial approximations to the exponential either introduce constant terms like the one above, or consist of functions which have singularities at $t = 0$. However, since the exponential thrust spin-up has a maximum torque early in the spin-up (decaying to zero) the errors associated with this form are less than those of constant torque, and the method presented here is conservative. Valid approximations to the exponential with the constant thrust method can be made. Hence, it may be concluded through some devious logic that N_z must be constant for a closed form solution of Eq. (16) and subsequent differential equations, and $\omega_z = \int N_z \, dt = N_z t$.

---

[8]If a digital solution of Eq. (16) and subsequent differential equations is used, any representation of N_z is allowable. The statements made here pertain to more "closed" solutions, in terms of known functions, which also require digital solutions, but can be easily generalized.

C. Wobble Error During Spin-Up

The angle at which the body-fixed roll axis wobbles about the angular momentum vector can now be determined. When N_z is constant and ω_{0z} is zero, then Eq. (16) is integrated to

$$\omega = \gamma N_z (1 + \lambda) e^{\frac{i\lambda N_z}{2} t^2} \int_0^t e^{\frac{-i\lambda N_z}{2}\tau^2} d\tau + \omega_0 e^{\frac{i\lambda N_z}{2} t^2}$$

(17)

where $\omega_0 = \omega_{0x} + i \omega_{0y}$, and $0 \leq t \leq t_1$ (torque time) is the running variable. The integral in Eq. (17) is a Fresnel integral, the results of which have been tabulated after the proper change of variable (Refs. 3 through 7).

The angular velocity vector, Ω, may then be written in body coordinates

$$\Omega = \omega_x \, i + \omega_y \, j + \omega_z \, k \, ,$$

where $\omega_x = \mathcal{R}_e \, \omega$, $\omega_y = \mathcal{I}_m \, \omega$ from Eq. (17), and $\omega_z = N_z t$. When $t = t_1$ (the upper limit on torque time), ω will assume the value attached to Eq. (17) when t_1 is substituted for t, and $\omega_z = N_z t_1 = s_0$ (the final spin rate), a design quantity which is sure to be known. The angular momentum vector is then $J = I \, \Omega$, where I is the column matrix $I^T = (I_x \, I_y \, I_z)$. Figure 3 shows the relationship among the body z-axis
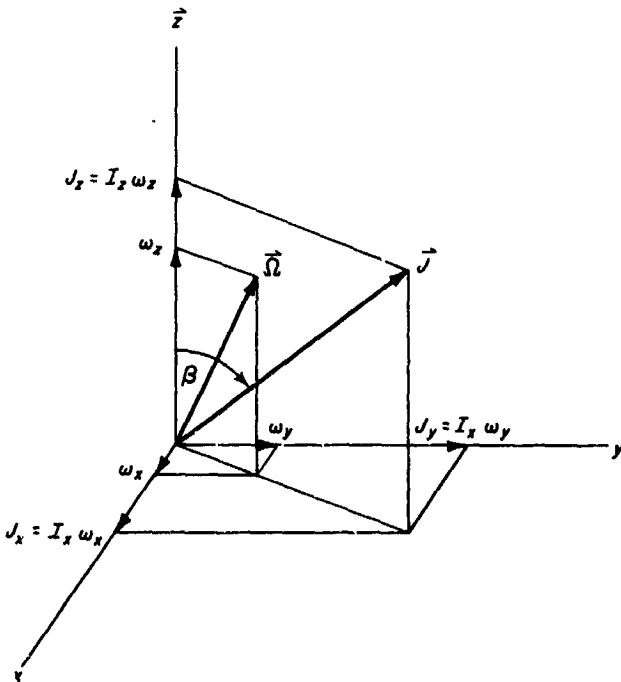
Fig. 3. Wobble angle, β

(spin), Ω and J. When $t = t_1$ and all external torques have ceased, J is invariant in space while the spin-axis z and the angular velocity vector Ω coplanar with J and z rotate about J at an angular rate $\frac{1}{2} \lambda N_z t_1^2$. The angle β, which is the wobble angle between z and J is seen to be

$$\tan | \beta | = \frac{\sqrt{J_x^2 + J_y^2}}{J_z^2} = \frac{I_x | \omega}{I_z \, s_0}$$

or, letting $\tan | \beta | \approx | \beta |$,

$$| \beta | = \frac{| \omega |}{(1 + \lambda) s_0}$$

(18)

In complex form, Eq. (18) is

$$\beta = \frac{\omega}{(1 + \lambda) s_0} \, ,$$

which is seen to be upon expansion using Eq. (17) ($t = t_1$).

$$\beta = \frac{\gamma N_z}{s_0} e^{\frac{i\lambda N_z}{2} t_1^2} \int_0^{t_1} e^{\frac{-i\lambda N_z}{2}\tau^2} d\tau + \frac{\omega_0}{(1+\lambda) s_0} e^{\frac{i\lambda N_z}{2} t_1^2}$$

Letting

$$K_1 = \frac{N_z}{s_0} e^{\frac{i\lambda N_z}{2} t_1^2} \int_0^{t_1} e^{\frac{-i\lambda N_z}{2}\tau^2} d\tau$$

(19)

and

$$K_2 = \frac{1}{(1+\lambda) s_0} e^{\frac{i\lambda N_z}{2} t_1^2}$$

(20)

then

$$\beta = \gamma K_1 + \omega_0 K_2$$

(21)

where K_1 and K_2 are functions of the shape of the rigid body (λ) and of specific spin-up values (N_z and t_1), but are independent of the error producing parameters γ and ω_0.

Looking at Eq. (18) again,

$$| \beta | = \left| e^{\frac{i\lambda N_z}{2} t_1^2} \right| \cdot \left| \frac{\gamma N_z}{s_0} \int_0^{t_1} e^{\frac{-i\lambda N_z}{2}\tau^2} d\tau + \frac{\omega_0}{(1+\lambda) s_0} \right|$$

$$| \beta | = \left| \frac{\gamma N_z}{s_0} \int_0^{t_1} e^{\frac{-i\lambda N_z}{2}\tau^2} d\tau + \frac{\omega_0}{(1+\lambda) s_0} \right|$$

(22)

Equation (22) is the form of the wobble angle which shall be used. The $| \beta |$ given in Eq. (22) is the initial condition for the thrusting phase (to be discussed in Section IV).

D. Inertial Displacement of J During Spin-Up

The angle through which J moves with respect to the inertial X_0-Y_0-Z_0 axes is now determined. Recall that Z_0 and z are coincident at $t = 0$. When torquing begins, J builds up from 0, wobbles about Z_0, then when $t = t_1$, J comes to rest at angle a_I from Z_0. Consequently, when determining a_I, the inertial transformation defined in Section II is needed. Using the value of ω found in Eq. (17) in the inertial Eq. (9),

$$\dot{a} + iN_z t a = \gamma N_z (1+\lambda) e^{\frac{i\lambda N_z}{2} t^2} \int_0^t e^{\frac{-i\lambda N_z}{2} \tau^2} d\tau$$

$$+ \omega_0 e^{\frac{i\lambda N_z}{2} t^2}$$

the solution of which is

$$a e^{\frac{iN_z}{2} t^2} = a_0 + K_3 \gamma + K_4 \omega_0 \tag{23}$$

where

$$K_3 = N_z (1+\lambda) \int_0^t e^{\frac{i(1+\lambda)N_z}{2} \tau^2} \left\{ \int_0^\tau e^{\frac{-i\lambda N_z}{2} \zeta^2} d\zeta \right\} d\tau \tag{24}$$

and

$$K_4 = \int_0^t e^{\frac{iN_z(1+\lambda)}{2} \tau^2} d\tau \tag{25}$$

The integration in K_4 is seen to be of the same form as the integral in K_1 (Eq. 19), i.e., a Fresnel integral.

Then, from Eq. (10)

$$a_I = a e^{i\int \omega_z dt} = a e^{i\int N_z t dt} = a e^{\frac{iN_z}{2} t^2}$$

and Eq. (23) becomes

$$a_I = a_0 + K_3 \gamma + K_4 \omega_0 \tag{26}$$

Since at $t = 0$, z and Z_0 are coincident, $a_0 = 0$. However, for an overall analysis, it must be remembered that $a_0 = \Theta_0 + \dot{\theta}_0 \delta t$ (discussed in the Introduction).

E. Combination of Body-Fixed and Inertial Errors

If the spin-up error is to be considered by itself, i.e., not used as an initial condition for some maneuver after spin-up, then the error in the angular momentum vector a_I is considered the prime error (β being a wobble superimposed on a_I). However, if a maneuver is to be performed

after spin-up (e.g., thrusting), then a_I and β must be combined in either of two ways:

1. If there is a coast period between the end of spin-up and start of maneuver, so that the position of s with respect to J may be considered random (i.e., s has precessed many times about J), then a_I and β are independent and treated as separate errors; i.e., a_I is the error incurred during spin-up and β is an initial condition imposed upon the subsequent maneuver.

$$|\epsilon|^2 = |a_I|^2 + |\beta|^2 \tag{27}$$

2. If the maneuver takes place immediately after spin-up, such that the position of s will be known with respect to J, then a_I and β must be vectorially added. In this case, the spin-up parameters must be well defined, and experimentation must agree with theory so that the directions of a_I and β in fact correspond to the analysis.

It will be shown later that the wobble rate $\dot{\phi} \approx (1+\lambda)s_0$, so that as $\lambda \to -1$ (a long thin rod spun about its axis of symmetry), $\dot{\phi}$ can become small, saying that s rotates very slowly about J, hence the direction might well be predicted. For the vectorial addition, refer to Fig. 4.
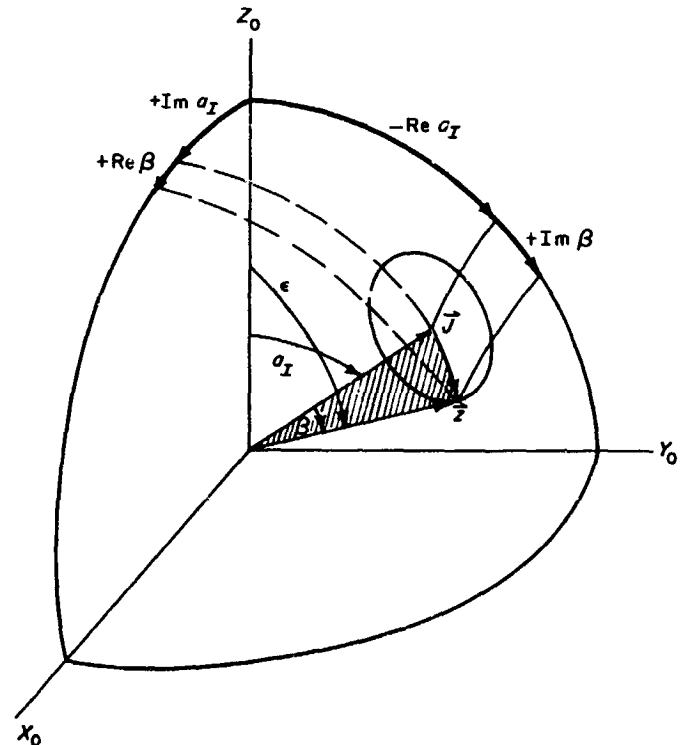

Fig. 4. Combination of a_I and β

Since $a_l = \theta (\cos \phi + i \sin \phi)$ when $\phi = 0$ (standing on the X_u axis), an observer sees $\mathcal{R}e\, a_l = \theta$, consequently it is just that component which is then projected onto the Y_u-direction (in this case $-\theta$, since θ is defined counterclockwise). The same is true for $\mathcal{I}m\, a_l$, but no sign change is required. β is defined in the normal way. Hence, in Fig. 4, a unit sphere is superimposed on the vector diagram, and the angular components are shown projected on the sphere. It can be seen that

$$\mathcal{I}_m \epsilon = \mathcal{I}_m \beta - \mathcal{R}_e a_l$$

$$\mathcal{R}_e \epsilon = \mathcal{R}_e \beta + \mathcal{I}_m a_l$$

whence

$$\epsilon = \beta - i a_l \qquad (28)$$

and $|\epsilon|$ is the required error.

A discussion of the errors defined above follows, with examples given for ϵ, β and a_l.

F. Discussion of Integrals

In order to solve numerically Eqs. (17) and (26), the quantities K_1, K_2, K_3 and K_4 must be evaluated. In all cases the variable is t where $0 \leq t \leq t_1$. As mentioned previously, K_1 and K_4 are Fresnel integrals, and the double integral in K_3 is the integral of a Fresnel integral. To get these integrals in familiar form, a change of variable is required. The usual argument in the exponent of the Fresnel integral is $i\pi u^2/2$. Hence, if this substitution is made in K_1, K_3 and K_4, they become

$$K_1(t_1) = \sqrt{\frac{\pi N_z}{\lambda s_0^2}}\, e^{\frac{i\lambda N_z}{2} t_1^2} \int_0^{\sqrt{\frac{\lambda N_z}{i}}\, t_1} e^{-\frac{i\pi}{2} u^2}\, du$$

$$K_3(t_1) = \pi \sqrt{\frac{1+\lambda}{\lambda}} \int_0^{\sqrt{\frac{N_z(1-\lambda)}{\pi}}\, t_1} e^{\frac{i\pi}{2} u^2} \int_0^{\sqrt{\frac{\lambda}{1+\lambda}}u} e^{-\frac{i\pi}{2} z^2}\, dx\, du$$

$$K_4(t_1) = \sqrt{\frac{\pi}{N_z(1+\lambda)}} \int_0^{\sqrt{\frac{N_z(1+\lambda)}{\pi}}\, t_1} e^{\frac{i\pi}{2} u^2}\, du$$

which can be verified by substitution. The final form of the K's is reached by getting rid of the clumsy design parameter N_z. Note that, for constant N_z,

$$N_z = s_0/t_1$$

Then, by substitution

$$\frac{1}{2} N_z t_1^2 = \frac{1}{2} s_0 t_1,$$

and the four K's assume their final form

$$K_1(t_1) = \sqrt{\frac{\pi}{\lambda s_0 t_1}}\, e^{\frac{i\lambda s_0 t_1}{2}} \int_0^{\sqrt{\frac{s_0 \lambda t_1}{\pi}}} e^{-\frac{i\pi}{2} u^2}\, du \qquad (29)$$

$$K_2(t) = \frac{1}{(1+\lambda) s_0}\, e^{\frac{i\lambda s_0 t_1}{2}} \qquad (30)$$

$$K_3(t_1) = \pi \sqrt{\frac{1+\lambda}{\lambda}} \int_0^{\sqrt{\frac{(1+\lambda) s_0 t_1}{\pi}}} e^{\frac{i\pi}{2} u^2} \int_0^{\sqrt{\frac{\lambda}{1+\lambda}}u} e^{-\frac{i\pi}{2} z^2}\, dx\, du \qquad (31)$$

$$K_4(t_1) = \sqrt{\frac{\pi t_1}{(1+\lambda) s_0}} \int_0^{\sqrt{\frac{s_0(1+\lambda) t_1}{\pi}}} e^{\frac{i\pi}{2} u^2}\, du \qquad (32)$$

When the shape of the body is stipulated, and the spin-up parameter s_0 is given, then the values of $K = f(t_1)$ may be determined, and the errors may be calculated with assumed values of γ and ω_0. As an illustration, Figs. 5 through 14 show the K's as functions of t_1 for a few combinations of λ and S_0.

The Fresnel integrals of K_1 and K_4 are of the following form (see, for example, Ref. 4):

$$C(v) = \int_0^v \cos \frac{\pi}{2} u^2\, du$$

$$S(v) = \int_0^v \sin \frac{\pi}{2} u^2\, du$$

where

$$E(v) = \int_0^v e^{\frac{i\pi}{2}u^2}\, du = C(v) + iS(v)$$

may be formed, and the conjugate of E is

$$\bar{E}(v) = \int_0^v e^{-\frac{i\pi}{2}u^2}\, du = C(v) - iS(v)$$

It is seen immediately that $C(0) = S(0) = 0$; however, $C(v)$ and $S(v)$ must be expanded asymptotically to determine

$$\lim_{t \to \infty} C(v) = \lim_{t \to \infty} S(v) = \frac{1}{2}$$

Reference 3 discusses briefly the nature and expansions of the Fresnel form in K_3. However, no tables of general parameters are known to exist. When the above properties of the Fresnel integral are applied to the K's, it may be deduced that

$$|K_1(t_1)| \leqslant 0.95 \sqrt{\frac{\pi}{\lambda s_0 t_1}} \tag{33}$$

$$|K_2(t_1)| \leqslant \frac{1}{s_0(1+\lambda)} \tag{34}$$

$$|K_3(t_1)| \leqslant k^\dagger \pi \sqrt{\frac{1+\lambda}{\lambda}} \tag{35}$$

$$|K_4(t_1)| \leqslant 0.95 \sqrt{\frac{\pi t_1}{(1+\lambda) s_0}} \tag{36}$$

where the constants are the maximum absolute values of the oscillating terms.

G. General Observations

The K's are bounded from Eqs. (33–36); therefore, the following conclusions (some obvious) may be drawn about the errors.

1. As t_1 increases, keeping s_0 constant,

---

†Where k is some finite number. This can be seen from Eq. (31), where the inner integral is a Fresnel integral, which is always bounded. This Fresnel integral is multiplied by a bounded sinusoid $e^{i\pi u^2/2}$ and integrated, the result of which must be bounded.

i | $K_1(t_1)$ | decreases, implying that the error contribution of the effective spin jet misalignment (γ) to the wobble angle (β) decreases as spin time t_1 increases.

ii | $K_4(t_1)$ | increases without bound, stating that the initial tip-off rate, ω_0, has had an increased time to act through, thus increasing a_i.

2. As the value of s_0 is increased, keeping t_1 constant, K_1, K_2, and K_4 decrease (K_3 not being affected). This indicates that s_0 should be as large as possible, which could be expected from the gyrodynamic effect of increased spin rate.

3. The quantity | $K_3(t_1)$ | is independent of t_1 and s_0 in its limiting condition (Eq. 35). K_3 contributes to the a_i error as amplified by γ. A physical interpretation of this is not immediately apparent.

4. All four K's are functions of the shape of the rigid body (λ).

5. As $t_1 \to 0$, the four K's reduce to (using L' Hospital's rule on K_1):

$$K_1(0) = 1$$

$$K_2(0) = \frac{1}{(1+\lambda) s_0}$$

$$K_3(0) = 0$$

$$K_4(0) = 0$$

which when substituted into the equations for a_i, β and then ϵ yield ($a_1 = 0$),

$$\epsilon = \beta = \gamma + \frac{\omega_0}{(1-\lambda) s_0} = \frac{J_z + J_x}{J_z} \tag{37}$$

which is immediately seen to be the rotation of J caused by the instantaneous application of the spin-jet misalignment, plus the initial tip-off component J_x/J_z.

Equation (37) can be used as a quick method of approximating total error. However, it should be remembered that this idealized case (i.e., $t_1 = 0$) is not conservative at all, and usually represents the lowest value attained. However, if t_1 is small, and an appropriate fudge factor is used, Eq. (37) is an "order of magnitude" approximation.

H. Limiting Cases

1. $\lambda = 0$ (sphere). The values for the K's are (using L'Hospital's rule on K_1 and K_3)

$$K_1 = 1$$

$$K_2 = 1/s_0$$

$$K_3 = i\left(1 - e^{\frac{i s_0 t_1}{2}}\right)$$

$$K_4 = \sqrt{\frac{\pi t_1}{s_0}}\ E\left\{\sqrt{\frac{s_0 t_1}{\pi}}\right\}$$

and the errors are

$$\beta = \gamma + \frac{\omega_0}{s_0}$$

$$a_I = i\gamma\left(1 - e^{\frac{i s_0 t_1}{2}}\right) + \omega_0 \sqrt{\frac{\pi t_1}{s_0}}\ E\left\{\sqrt{\frac{s_0 t_1}{\pi}}\right\}$$

$$\epsilon = \beta - i a_I = \epsilon_x + i\epsilon_y$$

$$\epsilon_x = \gamma\left(2 - \cos\frac{s_0 t_1}{2}\right) + \omega_0\left(\frac{1}{s_0} + \sqrt{\frac{\pi t_1}{s_0}}\ S\left\{\sqrt{\frac{s_0 t_1}{\pi}}\right\}\right)$$

$$\epsilon_y = -\gamma \sin\frac{s_0 t_1}{2} - \omega_0 \sqrt{\frac{\pi t_1}{s_0}}\ C\left\{\sqrt{\frac{s_0 t_1}{\pi}}\right\}$$

Notice that the $\sqrt{t_1}$ in the numerator of the second term of a_I makes ϵ divergent when $\omega_0 \neq 0$. As $t_1 \to 0$, $\epsilon = \beta$, the value of Eq. (37).

2. $\lambda = -1$ (thin rod). As $\lambda \to -1$, K_2 increases without limit (K_4 is finite because $(1 + \lambda)$ appears in the upper limit of the integral), the other K's being bound. This means that spinning-up a long thin rod about its symmetry axis ($I_z = 0$) when an initial tip-off rate is present, is highly unstable. This is intuitive in that if $I_z = 0$, there is no spin momentum to counteract the tumble of the rod.

3. $\lambda = +1$ (flat disc). As $\lambda \to +1$ (its maximum value), the coefficients of the K's are minimized, indicating that for a given spin-up time and rate, an infinitely flat disc is optimum. This is obvious from gyrodynamic considerations.

I. Initial Conditions

The relationship between the initial tip-off rate (ω_0 and $\dot\theta_0$) is found from Euler's rate transformations (Eq. 8)

$$\omega_x = \dot\phi \sin\theta \sin\psi + \dot\theta \cos\psi$$

$$\omega_y = \dot\phi \sin\theta \cos\psi - \dot\theta \sin\psi$$

$$\omega_z = \dot\phi \cos\theta + \dot\psi$$

Referring to Fig. 1, it may be stipulated that the initial conditions at $t = 0$ are

$$\phi = 0 \qquad \dot\phi = 0$$

$$\theta = 0 \qquad \dot\theta = \dot\theta_0$$

$$\psi = 0 \qquad \dot\psi = 0$$

which result in

$$\omega_{0x} = \dot\theta_0 \ ; \ \omega_{0y} = 0 \ ; \ \omega_{0z} = 0$$

where

$$\omega_0 = \omega_{0x} + i\,\omega_{0y} = \dot\theta_0.$$

Thus, it is being stated, without loss of generality, that whatever direction the tip-off occurs in, defines the X_0-Y_0 directions.

J. Numerical Evaluation of Errors

As mentioned in the Introduction, the two cases of interest in this Report are the Apollo-shaped capsule and the *Ranger* landing capsule. Since the K's need only the body shape λ and final spin rate s_0 to be evaluated, it was decided to keep the error sources $\dot\theta_0$ and γ strictly parametrical. Spin-up time (t_1) is taken with wide enough bounds to encompass most situations. The values used in determining the K's are the following:

	APOLLO	RANGER
λ	1/3	−3/4
Final spin rate, rad/sec (s_0)	1, 2, 5, 10	30
Spin-up time, sec (t_1)	0–10	0–3

Plots of both the real and imaginary portions of K_1, K_2, K_3 and K_4 vs t_1 are given in Figs. 5–14.

The numerical evaluation of K_1, K_3 and K_4 was, at first, very frustrating. Fresnel integrals are known for their difficulty in approximating over a large range of arguments. However, the excellent orthogonal polynomial (Chebyshev) approximation given in Ref. 6 is satisfactory for K_1 and K_4, while the corresponding function-generating polynomials were of sufficient accuracy for K_3. Asymptotic expansions for Fresnel integrals and for integrals of Fresnel integrals are given in Ref. 4.

One numerical example should suffice in illustrating the use of the K's in Figs. 5–14. Recalling Eqs. (21), (26), and (28)

$$\beta = K_1 \gamma + K_2 \omega_0$$

$$a_I = K_3 \gamma + K_4 \omega_0$$

$$\epsilon = \beta - i a_I$$
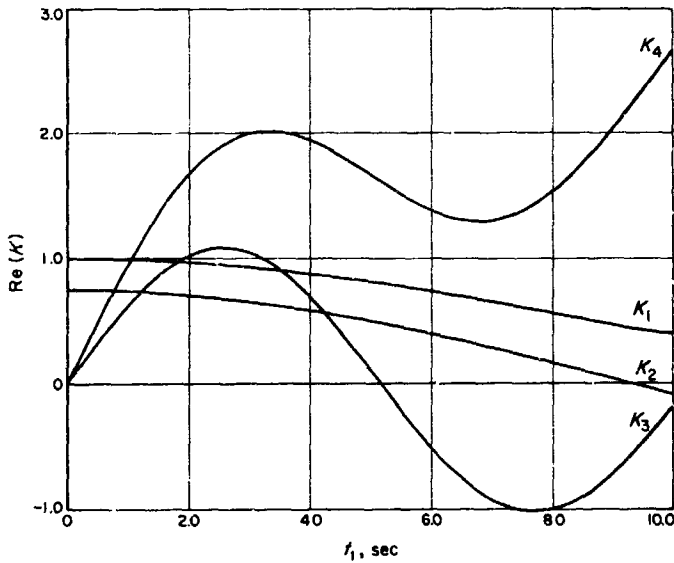
Fig. 5. Real parts of K_1, K_2, K_3 and K_4 vs t_1
$(s_0 = 1 \text{ rad/sec}, \lambda = + \frac{1}{3})$
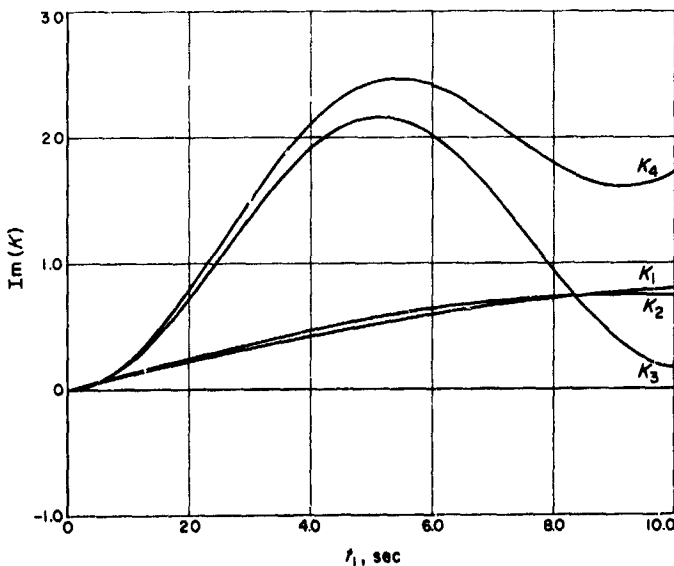
Fig. 6. Imaginary parts of K_1, K_2, K_3 and K_4 vs t_1
$(s_0 = 1 \text{ rad/sec}, \lambda = + \frac{1}{3})$
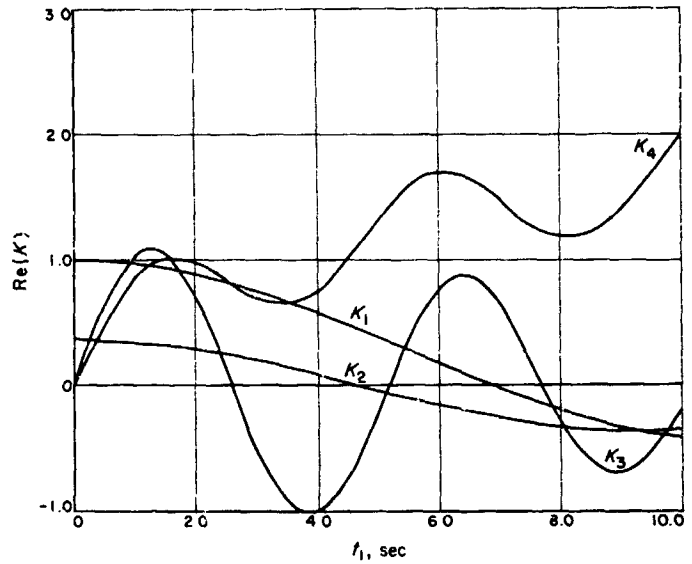
Fig. 7. Real parts of K_1, K_2, K_3 and K_4 vs t_1
$(s_0 = 2 \text{ rad/sec}, \lambda = + \frac{1}{3})$
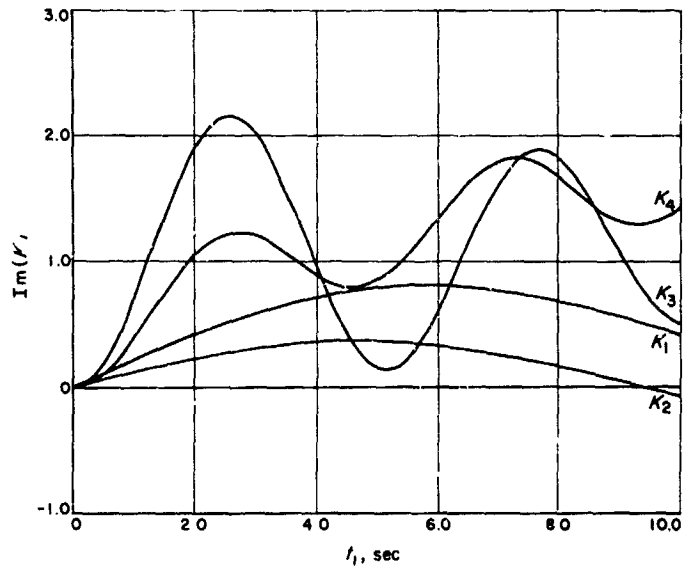
Fig. 8. Imaginary parts of K_1, K_2, K_3 and K_4 vs t_1
$(s_0 = 2 \text{ rad/sec}, \lambda = + \frac{1}{3})$

For *Ranger*, the specification for γ is 0.006 rad with a spin-up time of 1.0 sec.[9] If an initial tip-off rate of $\omega = \dot{\theta}_0 = 0.005$ rad/sec is assumed (realistic), then from Figs. 13 and 14,

[9]Aeronutronic Publication U-200, Final Technical Report—Lunar Rough Landing Capsule Development Program, Newport Beach, Calif., pp. 3–28.
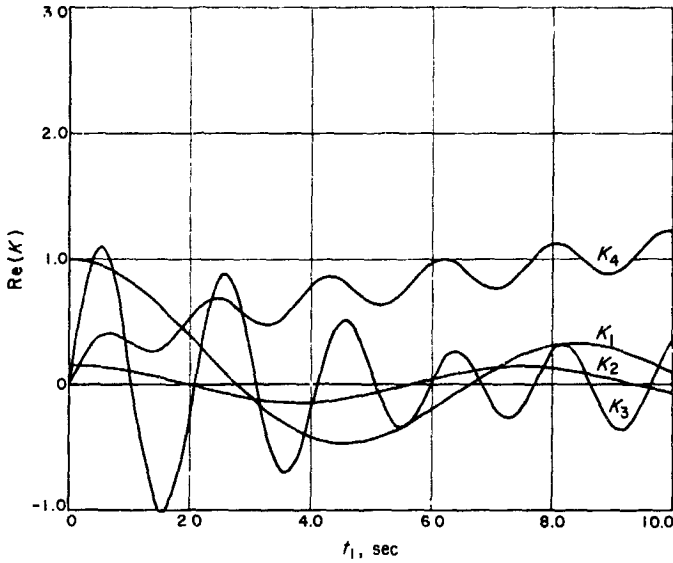
Fig. 9. Real parts of K_1, K_2, K_3 and K_4 vs t_1
$(s_0 = 5 \text{ rad/sec}, \lambda = + \frac{1}{3})$
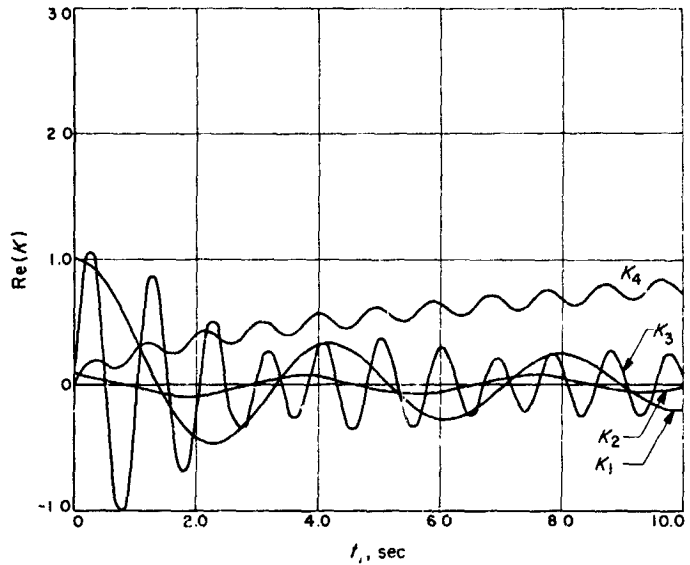
Fig. 11. Real parts of K_1, K_2, K_3 and K_4 vs t_1
$(s_0 = 10 \text{ rad/sec}, \lambda = + \frac{1}{3})$
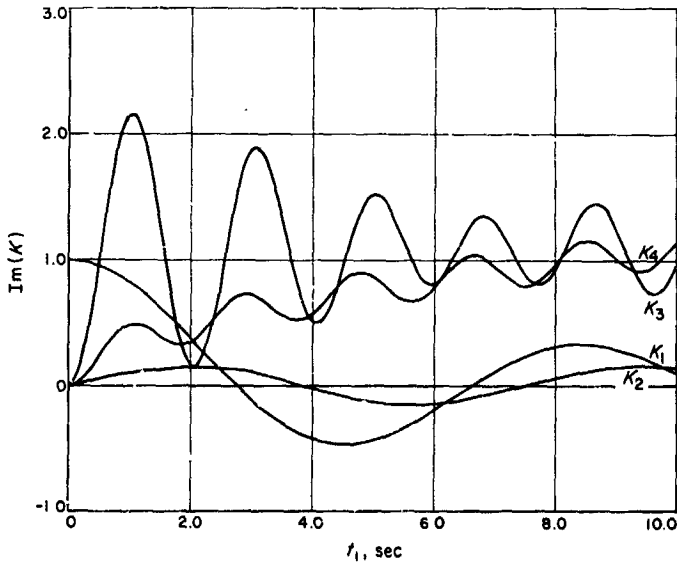
Fig. 10. Imaginary parts of K_1, K_2, K_3 and K_4 vs t_1
$(s_0 = 5 \text{ rad/sec}, \lambda = + \frac{1}{3})$
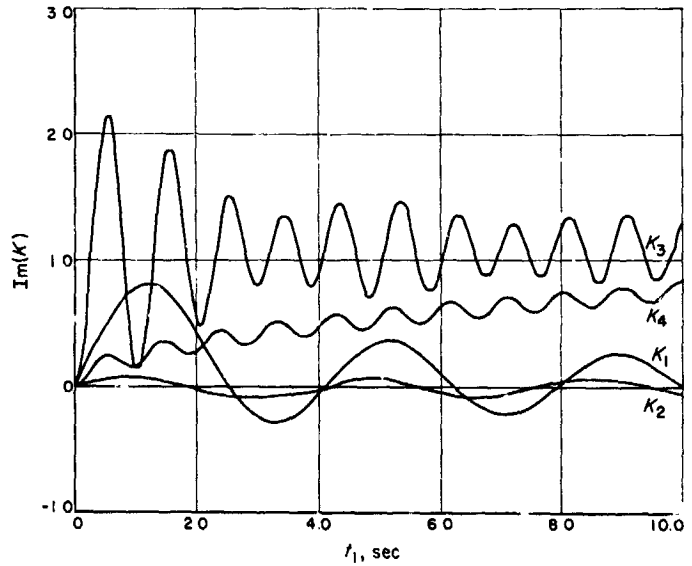
Fig. 12. Imaginary parts of K_1, K_2, K_3 and K_4 vs t_1
$(s_0 = 10 \text{ rad/sec}, \lambda = + \frac{1}{3})$

$$\mathcal{R}_e K_1 = - 0.208 \qquad \mathcal{R}_e K_2 = + 0.034$$
$$\mathcal{R}_e K_3 = - 0.238 \qquad \mathcal{R}_e K_4 = + 0.263$$
$$\mathcal{I}_m K_1 = + 0.094 \qquad \mathcal{I}_m K_2 = + 0.129$$
$$\mathcal{I}_m K_3 = + 0.671 \qquad \mathcal{I}_m K_4 = + 0.438$$

where

$$\beta = - 0.0011 + 0.0012\, i \text{ and } a_l = - 0.0001 + 0.0062\, i$$
$$\text{and } \epsilon = 0.005 + 0.001\, i \text{ and } |\epsilon| = 0.005 \text{ rad}$$
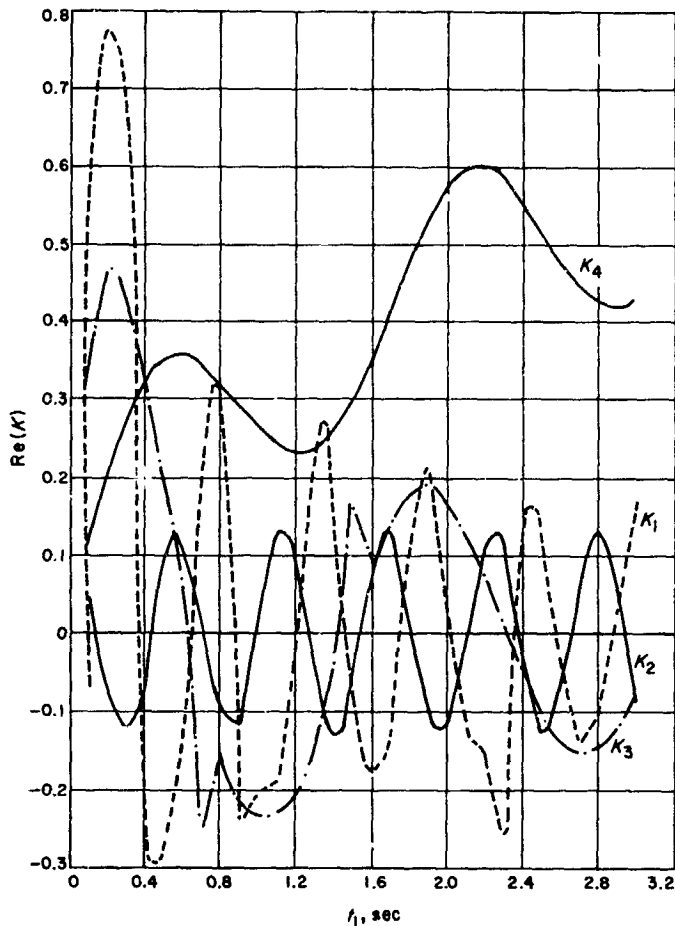
Fig. 13. Real parts of K_1, K_2, K_3 and K_4 vs t_1
(s_0 = 30 rad/sec, λ = — ¾)
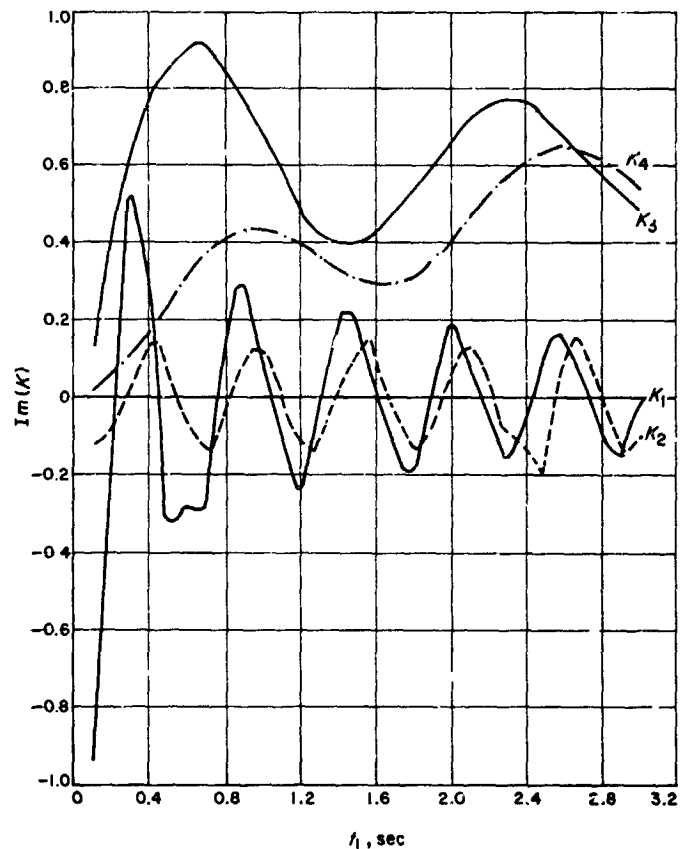
Fig. 14. Imaginary parts of K_1, K_2, K_3 and K_4 vs t_1
(s_0 = 30 rad/sec, λ = — ¾)

IV. THRUSTING OF SPINNING SYMMETRIC RIGID BODIES

A great deal of work has gone into analyzing the effects of rocket thrust misalignment on accelerated spinning bodies. References 4 and 8 are the classic works, done during the 1940's, primarily on spin-stabilized rockets launched from launchers with and without fins. The basic theory used in this Section is a combination of these and other referenced works. No claim is made to originality, except, perhaps Eq. 67.

The one design parameter which is common between the last Section and this Section (except shape of the body, λ) is the design spin rate s_0. An output of Section III, the wobble angle β_0, along with s_0, is used as an initial condition here. The inertial axes X_0-Y_0-Z_0 are redefined for this Section. When $t = 0$, the Z_0 axis coincides

with the angular momentum vector, J[10], and the Y_0 axis is along the direction of $-\beta_0$ (coinciding with the θ direction when $\phi = 0$; see Fig. 1).

First to be determined in this Section is the angle of attack, a_I, of the thrusted rigid body[11]. This inertial angle of attack defines the position of the thrust vector as a function of time. The thrust vector is then integrated

---

[10]Thus, the error between Z_0 and J of Section III, a_I, is subtracted out here. Of course, this error must be considered, and is discussed in Section VI.

[11]This a_I differs from that in Section III in that (a), this a_I is in a different time domain since the X_0,Y_0,Z_0 axes are redefined when $t = 0$ and (b), the a_I here includes wobble angle. Hence, $a_{I_0} = \beta_0$ when $t = 0$.

into velocity, and the resultant error in both the magnitude and direction is considered. There are certain simplifying assumptions made throughout this Section, such as constant mass, inertia, etc. A discussion of the effects of these assumptions is found in Appendix B.

A. Thrust Misalignment

Thrust misalignment, which can be defined as the lever arm through which a given thrust acts, gives the body both a rotational and a translational acceleration. The translational motion will be neglected in this Report since in nearly all applications of the dynamics described herein, such motion is second order. Therefore, the need for considering two separate types of thrust misalignment is avoided (see Fig. 15). If F is the thrust vector, constant with respect to the frame shown, δ the linear displacement of the point of thrust application (e.g., due to uneven rocket nozzle erosion), and α the angular misalignment (due to rocket nozzle misalignment), then the lever arm (ρ) through which F acts is seen to be (letting $\alpha \approx \sin \alpha$), $\delta + l\alpha$. If, however, an "effective thrust misalignment" angle ζ is defined such that $\zeta = \delta/l + \alpha$, then the lever arm is

$$\rho = l\,\zeta \tag{38}$$

which requires only the definition of the effective thrust misalignment angle, ζ. This assumption is allowable, since in the true definition of thrust misalignment, part of the α error went into translational motion which is neglected

here, and ρ, a measure of the misalignment, is estimated by ζ to the accuracy of small angle approximations. Appendix C contains data on the effective thrust misalignment from the 2nd and 3rd stages of the Scout launch vehicle. This data was used in the numerical evaluation.

It is also required that the thrust vector intersect the roll axis, i.e., no roll torque is present. If this is not the case, then nonconstant effects on spin rate during burning must be considered, which make the differential equations nonlinear (see Appendix B).

In determining the torque vector from Fig. 15,

$$F = F\,\zeta\,j + F\,k$$
$$r = -\,l\,k \tag{39}$$

whence torque

$$L = r \times F = l\,F\,\zeta\,i \tag{40}$$

which is all in the x-direction. As stated before, all the quantities constituting torque (l, F, ζ) are constant with time.

B. Body-Fixed Equations of Motion

Substituting the above torque into Euler's dynamical equations (3) gives

$$\dot{\omega} - i\,\lambda\,\omega\,\omega_z = \frac{l\,F\,\zeta}{I_x} = N \tag{41}$$

$$\dot{\omega}_z = \frac{L_z}{I_z} = 0 \tag{42}$$

Letting $\int \dot{\omega}_z\,dt = s_0$, the solution of Eq. (41) is

$$\omega = \left(\omega_0 - \frac{iN}{\lambda\,s_0}\right)e^{i\lambda s_0 t} + \frac{iN}{\lambda\,s_0} \tag{43}$$

where $\omega_0 = \omega_{0x} + i\omega_{0y}$ is discussed below.

The wobble angle, β, as a function of time, is given by Eq. (18) as

$$|\beta| = \frac{|\omega|}{(1 + \lambda)\,s_0} \tag{44}$$

Resolving Eq. (43) into components, noting that $\mathcal{I}_m\,N = 0$,

$$\omega_x = \mathcal{R}_e\,\omega = \omega_{0x}\cos \lambda s_0 t - (\omega_{0y} - N/\lambda s_0)\sin \lambda s_0 t$$

$$\omega_y = \mathcal{I}_m\,\omega = \omega_{0x}\sin \lambda s_0 t + (\omega_{0y} - N/\lambda s_0)\cos \lambda s_0 t + N/\lambda s_0$$

which reduce to (when time is eliminated)

$$\omega_x^2 + (\omega_y - N/\lambda s_0)^2 = \omega_{0x}^2 + (\omega_{0y} - N/\lambda s_0)^2 = R^2\,(\omega_0) \tag{48}$$

Fig. 15. Thrust misalignment angles
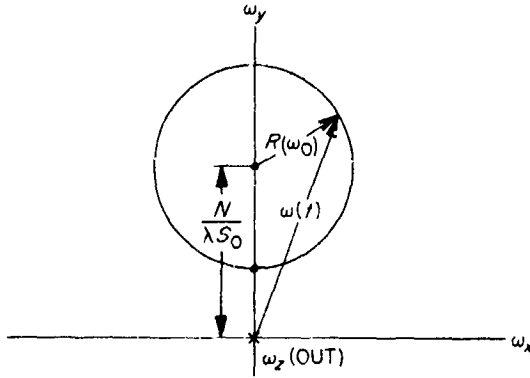
Fig. 16. Body-fixed rates of a symmetric body with torques

which is a circle with its center at $(0, N/\lambda s_0)$, and a radius of $R(\omega_0) = \{\omega_{0x}^2 + (\omega_{0y} - N/\lambda s_0)^2\}^{\frac{1}{2}}$. The complex radius vector, $\omega(t)$ rotates around the circle at an angular rate λs_0 (see Fig. 16). Since the coordinates are body-fixed, the angular momentum vector (J) and the angular velocity vector (Ω), which are coplanar with $\vec{\omega}_z$, rotate about the axis of symmetry of the body.

C. Initial Conditions

Certain relationships among the Eulerian angles need to be derived before initial conditions can be stipulated. Just before ignition of the rocket motor, the spinning body has no torques acting upon it, and the form in which the initial conditions appear must be determined. It is given that when $t = 0$, $\psi = \psi_0$, $\omega_{0z} = s_0$, $\theta = \theta_0 = \beta$ (from Section III), and $\dot{\phi} = \dot{\phi}_0$ (precession rate). Needed is $\omega_0 = \omega_{0x} + i\omega_{0y}$ in terms of the given quantities. Without loss in generality, the other Eulerian terms θ, ϕ, ψ are zero initially. The proofs that $\dot{\theta} = 0$ and $\dot{\phi} = \text{constant}$ will not be given here. The Eulerian angular transformations, Eqs. (8) are

$$\omega_{0x} = 0$$

$$\omega_{0y} = \dot{\phi}_0 \sin \theta_0 \approx \dot{\phi}_0 \theta_0 \qquad (49)$$

$$s_0 = \omega_{0z} = \dot{\phi}_0 \cos \theta_0 + \dot{\psi}_0 \approx \dot{\phi}_0 + \dot{\psi}_0$$

whereupon

$$\omega_0 = \omega_{0x} + i\omega_{0y} = i\dot{\phi}_0 \theta_0$$

Since it is the second order differential equations ($\dot{\omega} = d^2\xi/dt^2$, ξ some angular displacement) that are of interest, only two initial conditions must be stipulated (s_0, θ_0). Hence, some relationship must exist between $\dot{\phi}_0$ and s_0 and θ_0. This can be found by eliminating ω in Eqs. (4) and (8a) when $t = 0$ and $N = 0$ and initial conditions exist.

$$\dot{\omega} - i\lambda\omega\omega_z = N = 0 \qquad (4)$$

$$\omega = (\dot{\theta} + i\dot{\phi}\sin\theta)\,e^{-i\psi} \qquad (8a)$$

Taking the time derivative of Eq. (8a) and inserting the initial conditions, i.e., $\theta = \theta_0$, $\dot{\phi} = \dot{\phi}_0$, $\dot{\psi} = \dot{\psi}_0$, $\ddot{\theta} = 0$, $\ddot{\phi} = 0$, and $\psi = 0$,

$$\dot{\phi}\sin\theta_0\,(\dot{\psi}_0 + \lambda\,\omega_{0z}) = 0 \qquad (50)$$

which has roots of $\dot{\phi} = 0$, $\theta_0 = 0$ and $\dot{\psi}_0 = -\lambda\,\omega_{0z}$. If $\theta_0 = 0$, there are no initial conditions (since there is no wobble). If $\theta_0 \neq 0$, which necessarily implies that $\dot{\phi}_0 \neq 0$, then $\dot{\psi}_0 = -\lambda\omega_{0z}$ for Eq. (50) to hold, and when this value for $\dot{\psi}_0$ is substituted into Eq. (49),

$$\dot{\phi}_0 = \frac{(1 + \lambda)\,s_0}{\cos\theta_0} \qquad (51)$$

and Eq. (49) becomes

$$\omega_0 = \dot{\phi}_0\,\theta_0 = i\,(1 + \lambda)\,s_0\,\theta_0 \qquad (52)$$

for small θ_0.

D. Complete Inertial Transformation

Now the value for a_I (the inertial angle of attack) can be determined. Equation (9) stated that $\dot{a} + i\,s_0\,a = \omega$, and when the value for ω (found in part B) is substituted and the differential equation is solved, the result is

$$a\,e^{is_0t} = a_0 + \left\{\frac{i\omega_0}{s_0(\lambda + 1)} + \frac{N}{s_0^2\,\lambda(\lambda+1)}\right\}\left\{1 - e^{i(\lambda+1)s_0t}\right\}$$
$$- \frac{N}{\lambda s_0^2}\left\{1 - e^{is_0t}\right\} \qquad (53)$$

and from Eq. (10),

$$a_I = a\,e^{i\int\omega_t dt} = a\,e^{is_0t}$$

Letting $\omega_0 = i\,(1 + \lambda)\,s_0\,\theta_0$ and $a_0 = a_{I0} = \theta_0$, Eq. (53) becomes

$$a_I = \theta_0 + \left\{\frac{N}{s_0^2\,\lambda(\lambda+1)} - \theta_0\right\}\left\{1 - e^{i(\lambda+1)s_0t}\right\}$$
$$- \frac{N}{\lambda s_0^2}\left\{1 - e^{is_0t}\right\} \qquad (54)$$

Without going into too much detail at this point of the development, it can be seen that a_I is the sum of two sinusoids of differing amplitudes and frequencies. The frequency s_0 is the spin frequency, and $(1 + \lambda)\,s_0$ is seen

from Eq. (51) to be $\dot{\phi}_0$, or the initial precession rate if $\cos \theta_c \approx 1$. The amplitude of the first term can go to zero if N counteracts the wobble angle, θ_w. However, this only nulls the amplitude to the precession part, and does not cause a_i to go to zero. If $\theta_0 = 0$, the amplitudes of the two sinusoidal terms differ by a factor of $(\lambda + 1)$, which is bounded by 0 and 2. It will be seen later that if $\theta_0 \neq 0$, then it can become a predominate term.

E. Inertial Thrust Vector

Since the inertial angle of attack (a_i) is now known with respect to body-fixed parameters, the motion of the thrust vector in inertial space can be determined. The tool needed is the full Eulerian angular transformation. Rewriting the rotation matrices (see Fig. 1),

$$[\phi] = \begin{bmatrix} \cos \phi & \sin \phi & 0 \\ -\sin \phi & \cos \phi & 0 \\ 0 & 0 & 1 \end{bmatrix};$$

$$[\theta] = \begin{bmatrix} 1 & 0 & 0 \\ 0 & \cos \theta & \sin \theta \\ 0 & -\sin \theta & \cos \theta \end{bmatrix};$$

$$[\psi] = \begin{bmatrix} \cos \psi & \sin \psi & 0 \\ -\sin \psi & \cos \psi & 0 \\ 0 & 0 & 1 \end{bmatrix}$$

Then the operation of $[\psi] \cdot [\theta] \cdot [\phi] = \Gamma$ on any inertial vector will transform the same vector into body-fixed coordinates, or conversely

$$A_{\text{inertial}} = \Gamma^{-1} A_{\text{body-fixed}} = [\phi]^{-1} \cdot [\theta]^{-1} \cdot [\psi]^{-1} A_{\text{body-fixed}} \tag{55}$$

where the matrix multiplication yields

$$\Gamma^{-1} = \begin{bmatrix} \cos \phi \cos \psi - \cos \theta \sin \phi \sin \psi \\ \sin \phi \cos \psi + \cos \theta \sin \psi \cos \phi \\ \sin \theta \sin \psi \end{bmatrix}$$

$$\begin{matrix} -\cos \phi \sin \psi - \cos \theta \cos \psi \sin \phi & \sin \phi \sin \theta \\ -\sin \psi \sin \phi + \cos \theta \cos \phi \cos \psi & -\cos \phi \sin \theta \\ \sin \theta \cos \psi & \cos \theta \end{matrix} \tag{56}$$

Since Γ^{-1} is orthogonal, i.e., $|\Gamma^{-1}| = 1$, the inverse of the matrix is equal to its transpose. The body-fixed thrust

vector (F) is given in Eq. (39). If a small angle approximation is made for θ, then the inertial thrust vector, F', resolved into its coordinates from Eq. (55) above, is

$$F'_x = - F \zeta (\cos \phi \sin \psi + \cos \psi \sin \phi) + F \theta \sin \phi$$

$$F'_y = - F \zeta (\sin \phi \sin \psi - \cos \phi \cos \psi) - F \theta \cos \phi$$

$$F'_z = F \zeta \theta \cos \psi + F \cos \theta \tag{57}$$

The $\cos \theta$ is retained in F'_z for later consideration.

If a complex inertial thrust vector is defined $F'_{xy} = F'_x + i F'_y$, then by substitution, it is found that

$$F'_{xy} = i F \left\{ \zeta e^{i(\phi+\psi)} - \theta e^{i\phi} \right\} \tag{58}$$

The exponent in the first term is determined from $(\cos \theta \approx 1)$

$$\int i \omega_z \, dt = i \int (\dot{\phi} \cos \theta + \dot{\psi}) \, dt = i (\phi + \psi) = s_0 t \tag{59}$$

and the second term is by definition (Eq. 11), a_i. Therefore,

$$F'_{xy} = i F \left\{ \zeta e^{i s_0 t} - a_i \right\} \tag{60}$$

The above equation is the desired form of the complex inertial thrust vector. It is seen that if the two error sources ζ and θ_0 are zero, $F'_{xy} = 0$.

Equation (57) gives the thrust in the Z_0 direction. The first term $(F \zeta \theta \cos \psi)$ is the product of two small angles $(\zeta$ and $\theta)$ times a sinusoid, which, when integrated into velocity, will average zero. Hence, the very good approximation

$$F'_z = F \cos \theta \tag{61}$$

is made.

Depending on how F'_z is used, $\cos \theta$ can or cannot equal unity. If the change in the velocity due to the effects of thrust misalignment and initial conditions is required, then the small angle approximation should not be employed. However, if angular errors are of prime interest (as they are in this study), then little inaccuracy is incurred by letting $\cos \theta = 1$.

F. Velocity Vector

Velocity can be determined from the value of the inertial thrust vector. The velocity vector is defined in the same way as the thrust vector, i.e., one component along

the inertial Z_0 axis, the other component defined in the complex cross plane.

$$v'_{xy} = \frac{g}{\bar{m}} \int_0^t F'_{xy} \, dt$$

$$v'_z = \frac{g}{\bar{m}} \int_0^t F'_z \, dt \tag{62}$$

where $\bar{m}$ is the average mass of the body during thrusting and $g = 32.2$ ft/sec^2. If mass cannot be assumed constant, then the integration of Eq. (62) must be done numerically.

Then, from Eqs. (60) and (62),

$$v'_{xy} = \frac{g}{\bar{m}} \int_0^t i F \left\{ \zeta e^{is_0 t} - a_i \right\} dt$$

which is, when a_i (Eq. 54) is substituted and integrated,

$$v'_{xy} = \frac{igF}{\bar{m}} \left\{ -\frac{i\zeta}{s_0}(e^{is_0 t} - 1) \right.$$

$$-\frac{iA}{s_0(1+\lambda)}(e^{is_0(1+\lambda)t} - 1)$$

$$+ \left. \frac{iB}{s_0}(e^{is_0 t} - 1) - (A - B - \theta_0) \right\}$$

where, temporarily,

$$A = \frac{N}{\lambda(\lambda+1)s_0^2} - \theta_0 \text{ and } B = \frac{N}{\lambda s_0^2}$$
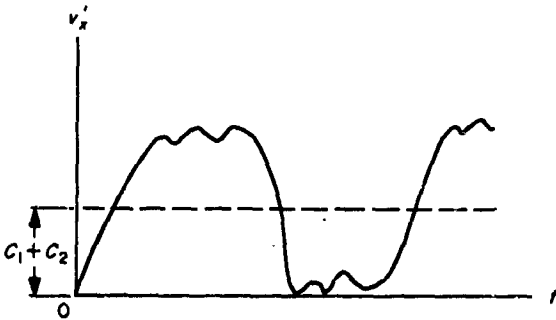
then reducing,

$$v'_{xy} = \frac{gF}{\bar{m}} \left\{ \left[\frac{\zeta}{s_0} - \frac{N}{\lambda s_0^3}\right]\left[e^{is_0 t} - 1\right] \right.$$

$$+ \left[\frac{N}{\lambda(\lambda+1)^2 s_0^2} - \frac{\theta_0}{(\lambda+1)s_0}\right]\left[e^{is_0(1+\lambda)t} - 1\right]$$

$$+ \left. \frac{itN}{(1+\lambda)s_0^2} \right\} \tag{63}$$

Equation (63) is the desired form of the cross velocity. Breaking v'_{xy} into its coordinates reveals its character.

$$v'_x = \mathcal{R}e \, v'_{xy} = C_1 \cos s_0 t + C_2 \cos s_0(1+\lambda)t - (C_1 + C_2)$$

$$v'_y = \mathcal{I}m \, v'_{xy} = C_1 \sin s_0 t + C_2 \sin s_0(1+\lambda)t + C_3 t$$

where the C's are the constants in Eq. (63). The above are seen to be modulated sinusoids, the first with a constant bias, $-(C_1 + C_2)$, and the second with a ramp function $(C_3 t)$ impressed over it. The general form of v'_x and v'_y is shown in Fig. 17. In the plots, either $\lambda \approx -1$ and $C_2 \gg C_1$ or $\lambda \approx +1$ and $C_1 \gg C_2$. If $\lambda \approx 0$, the qualitative solution shown is not valid.

Plots of v'_x vs v'_y are shown in Appendix B. These corroborate the cross-plotting of Fig. 17.

If $\cos \theta \approx 1$, the integration of v'_z is straightforward.

$$v'_z = \frac{g}{\bar{m}} \int_0^t F'_z \, dt = \frac{g}{\bar{m}} \int_0^t F \, dt = \frac{Fg}{\bar{m}} t \tag{64}$$

(a)

(b)

Fig. 17. Shape of cross velocities V_x and V_y

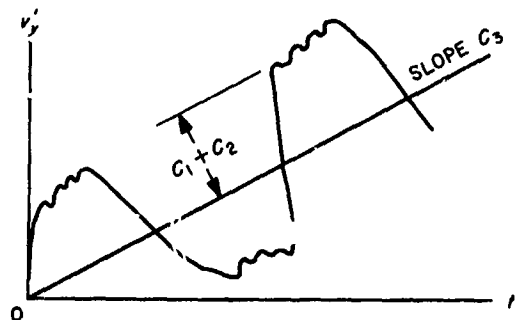However, if the small angle approximation cannot be made, i.e., the change in v'_z is desired, then

$$v'_z = \frac{g}{m}\int_0^t F\cos\theta\,dt = \frac{gF}{m}\int_0^t \cos|a_1|\,dt\ ,\quad (65)$$

and numerical integration is necessary.

G. Velocity Dispersion

If $v'_{xy} = 0$ due to the absence of initial conditions and thrust misalignments, then the resultant velocity would lie entirely upon the Z_0 axis. When $v'_{xy} \neq 0$, the tip of the resultant velocity vector is moved from the Z_0 axis (Fig. 18) at an angle

$$a = \tan^{-1}\frac{v'_{xy}}{v'_z} \approx \frac{v'_{xy}}{v'_z} \qquad (66)$$

a is seen to be the velocity dispersion angle caused by the presence of a cross velocity, v'_{xy} . The final value of a is reached when the time $t = t_b$, the burning time of the rocket motor.

Equation (66) is expanded to (with the use of Eqs. 63 and 64)

$$a(t) = \frac{1}{t}\left(\frac{\zeta}{s_0} - \frac{N}{\lambda s_0^3}\right)\left(e^{is_0 t} - 1\right)$$
$$+ \frac{1}{t}\left(\frac{N}{\lambda(\lambda+1)^2 s_0^2} - \frac{\theta_0}{(\lambda+1)s_0}\right)\left(e^{is_0(1+\lambda)t} - 1\right)$$
$$+ \frac{iN}{(1+\lambda)s_0^2}$$

$$(67)$$

It is seen from Eq. (67) that if $N = \lambda(\lambda + 1)s_0\theta_0$, the precession amplitude vanishes. The spinning amplitude can furthermore be nulled if the thrust misalignment $\zeta = \theta_0(1 + \lambda)/s_0$, but the bias term, $N/(1 + \lambda)s_0^2$, remains. Only if $\zeta = N = \theta_0 = 0$ does $a(t) = 0$ for all values of t.

Of prime interest is the magnitude of a, i.e., $|a| = (\mathscr{R}e^2 a + \mathscr{I}m^2 a)^{1/2}$. The radial direction of a with respect to the inertial system (angle η in Fig. 18) is of no interest
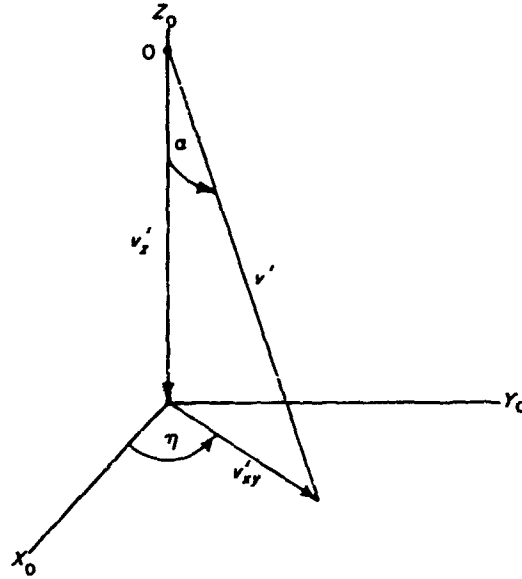
Fig. 18. Velocity dispersion angles

and is treated as a random variable because of the randomness of the θ_0 direction with respect to the true inertial system defined in Section VI. If it is required, it is seen from Fig. 18 to be $\tan^{-1}(v'_y/v'_x)$.

The wobble at the end of burn can be considered an output error. If this is denoted by β_1, then from Eqs. (43) and (44),

$$|\beta_1| = \frac{|\omega|}{(1+\lambda)s_0} = \theta_0 - \frac{N}{\lambda(\lambda+1)s_0^2} \qquad (68)$$

It is seen that if $-1 < \lambda < 0$, i.e., $I_z > I_z$, then the right term is negative and $|\beta_1| > \theta_0$. N itself is always defined positive (the worst case).

Another error which might be of interest (neglected here) is the error in the magnitude of the velocity vector (a is the error in direction). The value of v'_z is obtained from Eq. (65); the odd term appearing in Eq. (57) (i.e., $F_z \theta \cos\psi$) still being neglected. This v'_z is compared to the value of the velocity had the thrust always been applied along the Z_0 axis, $\Delta v_z = c\ln(m_i/m_f)$, c being the exhaust velocity of the gases, m_i the initial mass before thrusting and m_f the final mass when $t = t_b$; i.e., $m_i - m_f$ = mass of propellant expelled. The difference in magnitude of the two velocity vectors has been less than 1% for the range of parameters the author has dealt with. This means that the initial conditions and thrust misalignment cause less than 1% of the linear momentum of the rocket motor to be changed by spinning.

H. Limiting Cases

A close inspection of Eq. (67) yields the following information about α:

1. Taking limits on t

As t grows very large,

$$\lim_{t \to \infty} |\alpha| = \alpha_\infty = \frac{N}{(1+\lambda)s_0^2} = \frac{Fl\zeta}{I_z s_0^2} \qquad (69)$$

recalling that $N = Fl\zeta/I_r$. Hence, after t gets very large, α approaches a constant value which is inversely proportional to spin-rate squared, and directly proportional to acceleration (F/m). This can be a useful approximation if the body goes through enough revolutions, so that the amplitudes of the first two terms in Eq. (67) are small compared to α_∞. If the parameters are further broken down, it can be seen that $F = I_T/t_b$ where I_T is the total impulse of the rocket motor, and t_b is the burning time. I_T is a measure of the velocity requirement (since t_b is a motor parameter). When the above value for thrust is substituted into Eq. (69), the result is

$$\alpha_\infty = \left(\frac{I_T l\zeta}{I_z}\right)\frac{1}{s_0^2 t_b} \qquad (70)$$
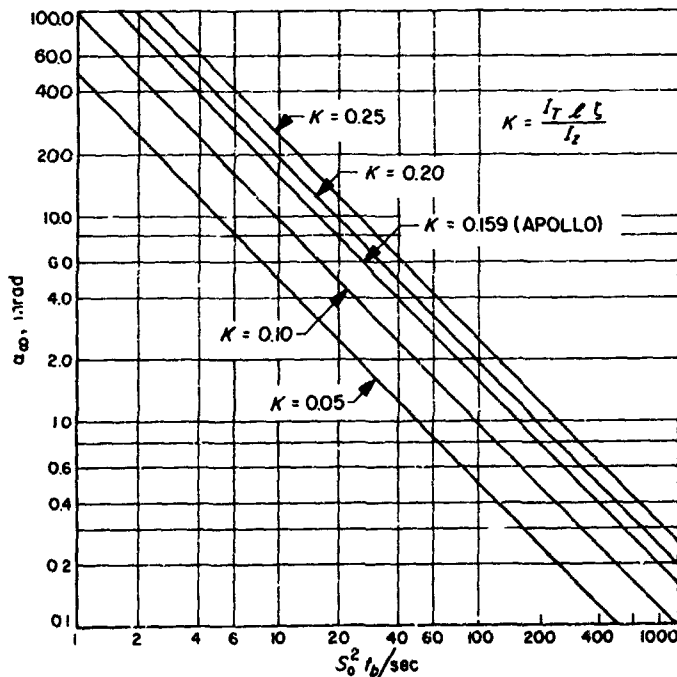

Fig. 19. α_∞ vs $s_0^2\ t_b$ for several values of K

Figure 19 is a plot of α_∞ vs $s_0^2\ t_b$ for several values of

$$\left(\frac{I_T\,l\,\zeta}{I_z}\right).$$

At the other extreme (as t grows small), after L'Hospital's rule is applied

$$\lim_{t \to 0}|\alpha| = \alpha_0 = |\zeta - \theta_0| \qquad (71)$$

which is evident from the position of the thrust vector at $t = 0$ with respect to the inertial Z_0 axis.

2. Taking limits on λ

As $\lambda \to 0$ (sphere), α blows up in both the first two coefficients (Eq. 67), as would be expected, since a sphere has no body-fixed gyrodynamic stability. However if $t \to \infty$ at the same time, the results of Eq. (69) are

$$\lim_{\lambda \to 0} \left\{ \lim_{t \to \infty} \alpha \right\} = \frac{N}{s_0^2};$$

the same result is obtained if the limits are taken in reverse order and L'Hospital's rule is applied. If $t \to 0$ as $\lambda \to 0$, from Eq. (71),

$$\lim_{\lambda \to 0} \left\{ \lim_{t \to 0} \alpha \right\} = |\zeta - \theta_0|$$

As $\lambda \to -1$ (thin rod), the second and third terms of Eq. (67) blow up and cause divergence of α. This also can be anticipated, since when $\lambda = -1$, $I_z = 0$, and there is no angular momentum generated along the z-axis to counteract the effect of thrust misalignment.

When $\lambda \to +1$ (flat disc), the three coefficients in Eq. (67) are minimized with respect to λ, thus minimizing $\alpha(t)$. This results from the maximum momentum developed in the z-direction.

3. Taking limits on s_0

If $s_0 \to 0$, a divergent form of Eq. (67) appears. This, however, is not indicative of the case since the small angle approximations no longer hold. Appendix D treats this special case.

As $s_0 \to \infty$, the resultant error $\alpha(t) \to 0$, since infinite stability is being approached.

I. Maximum Envelope of Solutions

If the constant coefficients in Eq. (67) are denoted K_1, K_2 and α_∞ respectively, i.e.,[†]

$$\alpha = \frac{K_1}{t}(e^{is_0 t} - 1) + \frac{K_2}{t}(e^{i(1+\lambda)s_0 t} - 1) + i\,\alpha_\infty$$

(72)

the real and imaginary components of α may be written as

$$\alpha_R = \mathscr{R}_e\,\alpha = \frac{K_1}{t}\cos s_0 t$$

$$+ \frac{K_2}{t}\cos s_0(1 + \lambda)t - \left(\frac{K_1 + K_2}{t}\right)$$

$$\alpha_I = \mathscr{I}_m\,\alpha = \frac{K_1}{t}\sin s_0 t$$

$$+ \frac{K_2}{t}\sin s_0(1 + \lambda)t + \alpha_\infty$$

(73)

If the maximum values of the sinusoids are chosen in such a way that if both $K_1 > 0$, $K_2 > 0$, or both $K_1 < 0$ and $K_2 < 0$, (α_∞ is always > 0), then

$$\alpha_R < \frac{\pm 2}{t}(K_1 + K_2)$$

$$\alpha_I < \frac{\pm 1}{t}(K_1 + K_2) + \alpha_\infty$$

(74)

or if $K_1 < 0$ while $K_2 > 0$, then,

$$\alpha_I < \frac{2}{t}(K_1^2 + K_2^2)^{1/2}$$

$$\alpha_R < \frac{1}{t}(K_2 - K_1) + \alpha_\infty$$

(74a)

The maximum magnitude of α will then be given by

$$|\alpha(t)| \leq (\alpha_R^2 + \alpha_I^2)^{1/2}$$

(75)

If Eq. (74) is substituted into Eq. (75), it is seen that $|\alpha(t)|$ is a fourth order polynomial which approaches a hyperbola as $\alpha_\infty \to 0$. The curve at the point $t = 0$ has a singularity, and thus must be mated to the $|\alpha(t)|$ axis at α_0. Figure 20 shows how the envelope of $|\alpha(t)|$ behaves.

[†]The K's used here are totally independent of those used in Section III, and are the result of an unfortunate choice of symbols.
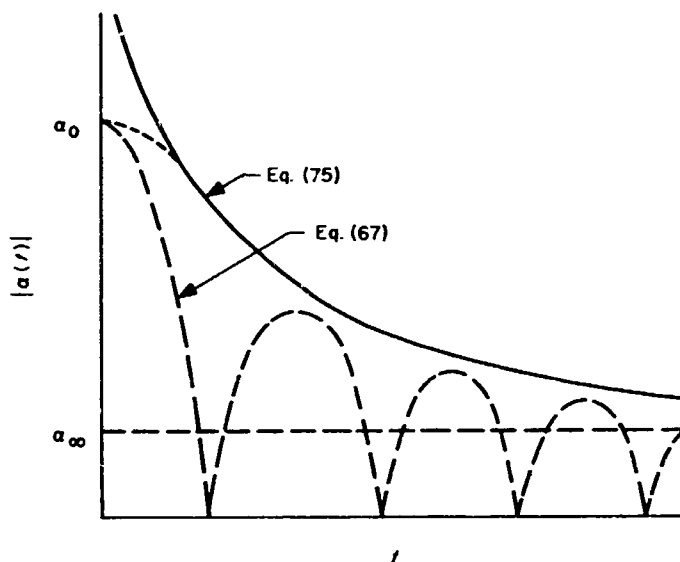
Fig. 20. Maximum envelope of solutions

The dashed lines are the real solution of $|\alpha(t)|$ in Eq. (67). It is to be noted that the body should go through at least 3 revolutions, i.e., $s_0 t_b/2\pi > 3$ for this envelope approximation to be valid.

J. Some Examples

A few examples are given of the results in this Section. The basic parameters will be the same as those of the last Section, i.e., Apollo and Ranger capsules, same spin-rate, etc. The error output of Section III is used as an input here (wobble angle θ_0). Table 1 lists the pertiment data. The results are shown in Figs. 21–27.

Table 1. Basic parameters

	Apollo	Ranger
K^*	+216.4	− 5,000, −10,000, −20,000
Thrust misalignment ζ, rad	0.004[†]	0.004[†]
Rocket burn time t_b, sec	5.0	9.6
Capsule shape λ	⅓	−¾
Initial spin rate, s_0, rad/sec	1 2 5 10	30
Initial wobble angle θ_0, rad	0.025 0.013 0.005 0.003**	0.001**

$^*K = \frac{t_b\,r\,\ell}{\lambda I_s}$, a catch-all term arising out of Eq. (67).

**Based on outputs of Section III.
[†]See Appendix C.

Fig. 21. $\alpha(t)$ vs t for Apollo-shaped capsule $s_0 = 1$ rad/sec, $\theta_0 = 0.025$ rad

Fig. 23. $\alpha(t)$ vs t for Apollo-shaped capsule $s_0 = 5$ rad/sec, $\theta_0 = 0.005$ rad

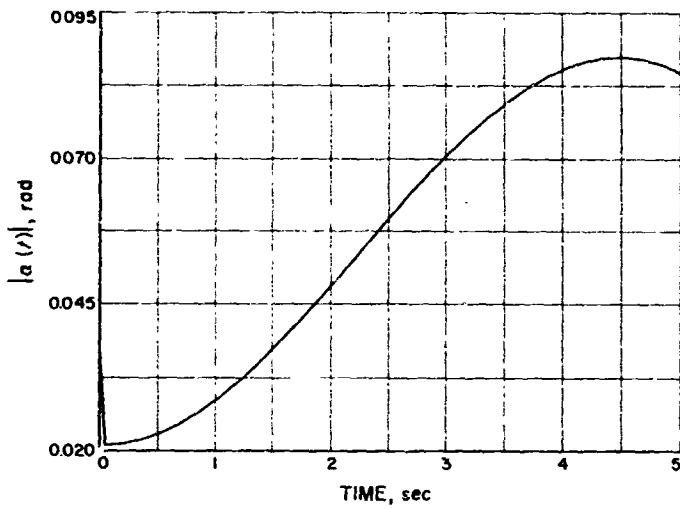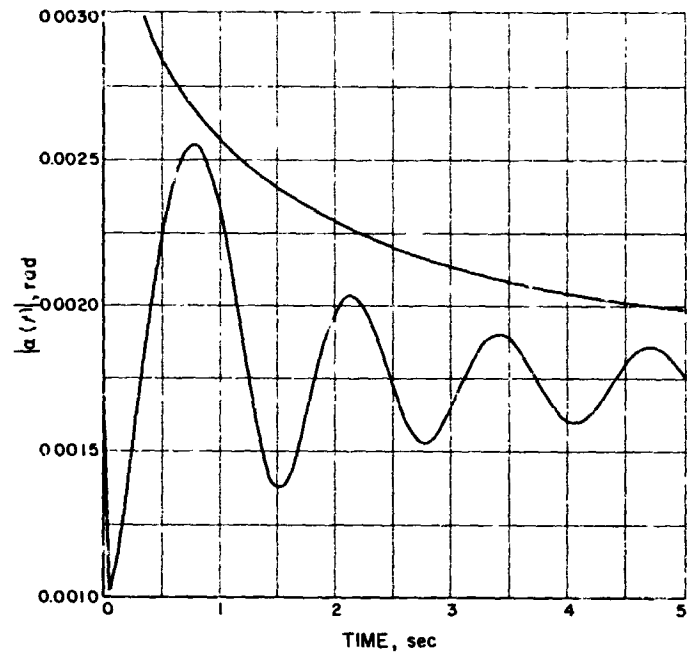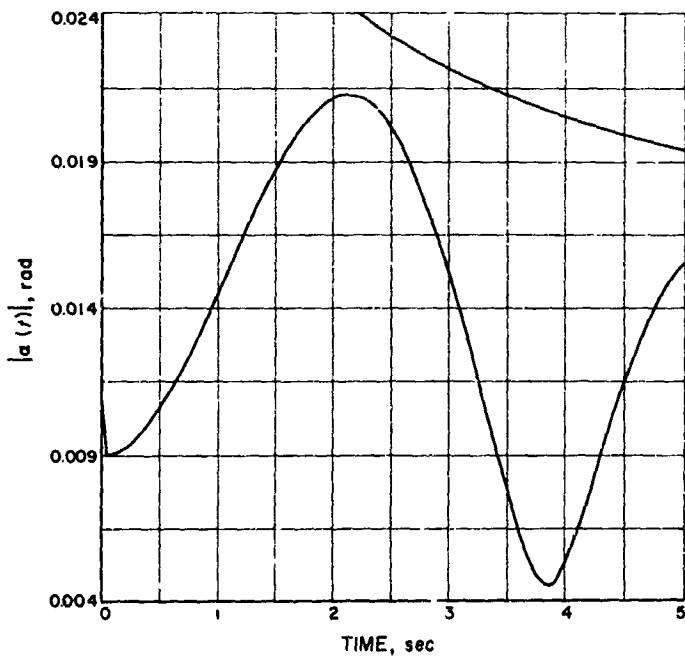**Fig. 22.** $\alpha(t)$ vs t for Apollo-shaped capsule $s_0 = 2$ rad/sec, $\theta_0 = 0.013$ rad
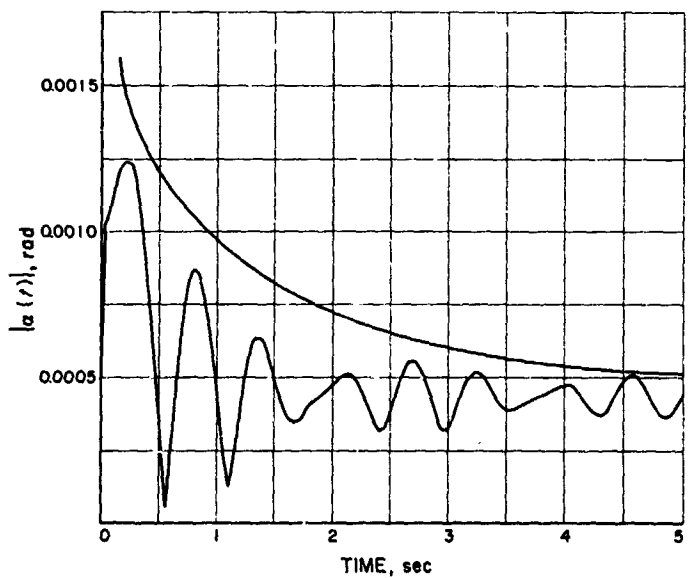
Fig. 24. $\alpha(t)$ vs t for Apollo-shaped capsule $s_0 = 10$ rad/sec, $\theta_0 = 0.003$ rad

Fig. 25. α (t) vs t for Ranger capsule K = — 5000

Fig. 26. α (t) vs t for Ranger capsule K = — 10,000
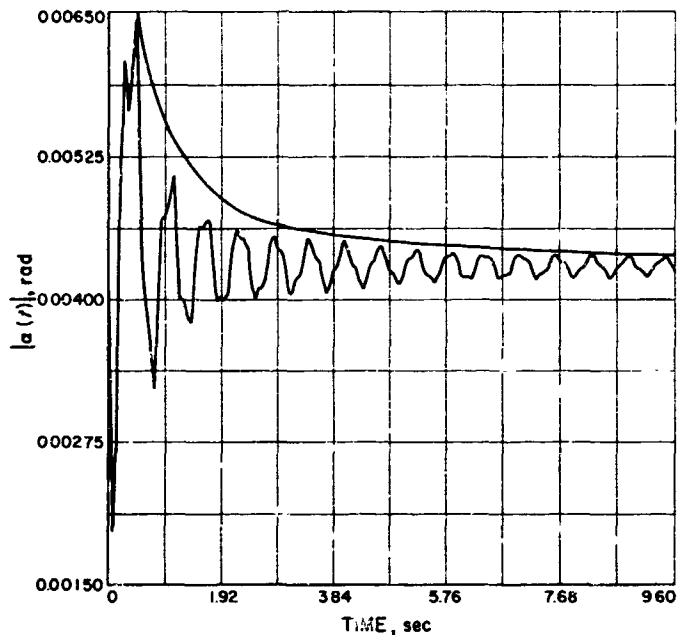
Fig. 27. α (t) vs t for Ranger capsule K = — 20,000

Three values of K are used for Ranger because of the large mass change involved during burning. In fact, the approximation for α (t) does not hold too well in cases such as this.

Superimposed on the results of Eq. (67) are the maximum envelope curves of Section IV, Part I. For the case of s_0 = 1.0 rad/sec, θ_0 = 0.025 rad (APOLLO), the envelope lies off the graph. As seen from the curves, the greater the value of s_0, the better the approximation.
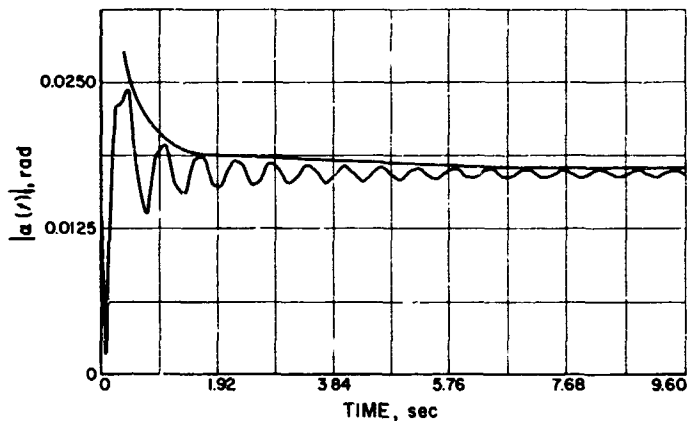
V. STABILITY OF NOT-SO-RIGID SPINNING BODIES

From classical rigid body dynamics it is known that a perfectly rigid rotating body is stable if it is spinning about the axis of either greatest or least inertia in torque-free space. If nonrigidity is present in the form of bending, sloshing, rubbing, etc., then spin about any axis except that of greatest inertia is unstable. This instability is in the form of a precession which causes fluctuating forces to dissipate energy in the nonrigid parts of the body until the spin is about the axis of greatest inertia.

When the Explorer I satellite was launched, the above phenomena was not taken into account, and the satellite (a cigar shaped body with long, flexible antennae extending from the center, perpendicular to the axis of symmetry) was found to change its axis of spin from that of symmetry (least inertia) to almost a transverse axis (greatest inertia) in 1½ hr. Subsequent analysis (Ref. 9) determined that the whip antennae served as ideal energy dissipators during precessional modes.

Other possible applications of spinning for inertial stability have brought this question to light. As will be seen later, this problem is an extremely difficult one to solve if obvious sources of nonrigidity are not present. As an example, the whip antennae were removed from the satellite for the *Explorer III* launch, and it took 10 days to wobble 75 deg. This rate is slow enough that a number of items might have caused or contributed to it.

This Section investigates the rate at which the angular velocity vector traverses from that of spin about an axis of minimum inertia to that of maximum inertia. The fluctuating acceleration on an element of mass is found, and a qualitative look at the effect of initial spin rate on wobble is made.

A. Dynamical Equations

Since the rotational energy is the coupling quantity between wobble angle θ and time,

$$\frac{d\theta}{dt} = \left(\frac{d\theta}{dT}\right)\left(\frac{dT}{dt}\right) \tag{76}$$

where T is the rotational kinetic energy. $d\theta/dT$ is easily derived from rigid body dynamics, whereas $\dot{T}$ is a more difficult term to find. The angular momentum vector remains invariant at J_0 regardless of the rotational energy variation (see Ref. 10). Figure 28 shows the position of J_0 with respect to the body-fixed axes x, y, z, and
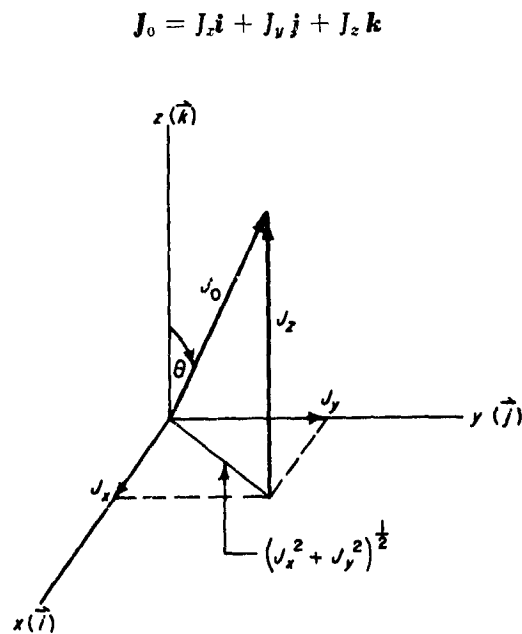
$$J_0 = J_x i + J_y j + J_z k$$

Fig. 28. Resolution of angular momentum vector

where i, j and k are the body-fixed unit vectors. For a body of revolution about the z axis,

$$J_x = I_x \omega_x \quad , \quad J_y = I_x \omega_y \quad , \quad J_z = I_z \omega_z$$

and the rotational energy is

$$T = \frac{I_x}{2}\left(\omega_x^2 + \omega_y^2\right) + \frac{I_z}{2}\omega_z^2 = \frac{1}{2I_x}\left(J_x^2 + J_y^2\right) + \frac{1}{2I_z}J_z^2 \tag{77}$$

and from Fig. 28:

$$J_x^2 + J_y^2 = J_0^2 \sin^2 \theta$$

$$J_z^2 = J_0^2 \cos^2 \theta \tag{78}$$

where $J_0 = I_z s_0$ and is constant. Equations (77) upon substitution and rearranging, become

$$\frac{2T}{J_0^2} = \frac{\sin^2 \theta}{I_x} + \frac{\cos^2 \theta}{I_z} = \frac{1}{I_x} + \left(\frac{1}{I_z} - \frac{1}{I_x}\right)\cos^2 \theta$$

If energy is dissipated, θ must increase as T decreases, which implies that $I_x > I_z$ for a real solution. This confirms what was said before, that the system is tending toward the axis of highest inertia.

If both sides of Eqs. (77) are divided by the initial rotational energy $(T_0 = I_z s_0^2/2)$, and the ratio T/T_0 is defined as T_r, then

$$T_r = 1 + \lambda \sin^2 \theta \tag{79}$$

where $\lambda = I_z/I_x - 1$. This equation is of marked interest in that it states that the way in which the kinetic energy decreases is only dependent upon the shape of the body (λ) and the wobble angle (θ). This fact will be used later in determining the effect of initial spin on $\dot{\theta}$. Equation (79) is plotted on Fig. 29.

The rate at which θ changes with respect to T_r is

$$\frac{d\theta}{dT_r} = \left[\frac{dT_r}{d\theta}\right]^{-1} = \frac{1}{\lambda \sin 2\theta}$$

$$= \frac{1}{2}\left\{\frac{1}{(T_r - 1)(\lambda + 1 - T_r)}\right\}^{\frac{1}{2}} \tag{80}$$

which is shown in Fig. 30. It is seen that $d\theta/dT_r$ has no real solution outside the limits $(1 + \lambda) < T_r < 1$. These bounds, of course, define the limits on the wobble angle θ, i.e., $T_r = 1 + \lambda$ is total stability $\theta = 90$ deg, and $T_r = 1$ is the condition when $\theta = 0$.
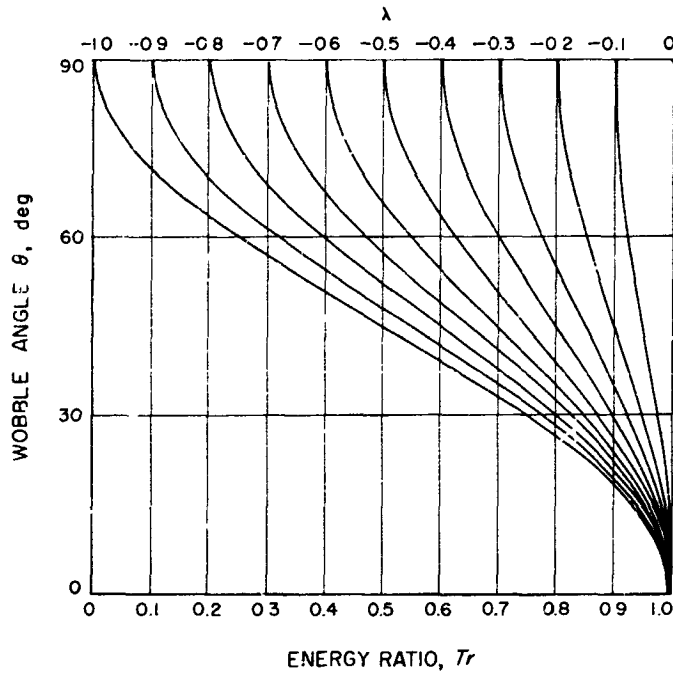
Fig. 29. Kinetic energy ratio vs wobble angle
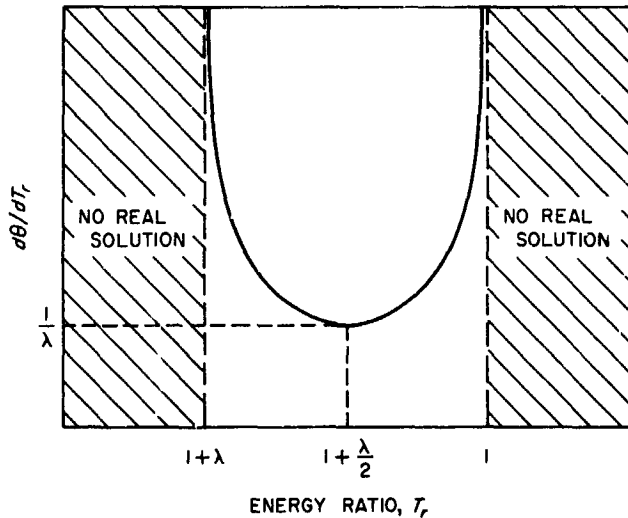
Fig. 30. Range of solutions for $d\theta/dT_R$

It is important to note that both the function $\theta = f(T_r)$ and its derivative $\theta' = d\theta/dT_r$ are asymptotic at the limits of T_r. Therefore, neither condition is ever really reached. If $\theta = 0$, i.e., $T_r = 1$, all acceleration is normal to the spin axis and no fluctuating forces are present. Hence, the body is stable. By the same token, as $\theta \to 90$ deg, the accelerations are approaching a constant magnitude from the other direction, which indicates that $\theta = 90$ deg is never reached, only approached. Therefore, when the wobble angle is said to be going from 0–90 deg, what

is really meant is that it goes from some initial[12] value θ_0 to some other value, which, in the case of *Explorer III*, was 75 deg for the 10-day number quoted.

The value of $d\theta/dT$, which is needed in Eq. (76), is then

$$\frac{d\theta}{dT} = \left[T_0 \frac{dT_r}{d\theta} \right]^{-1} = \frac{1}{T_0 \lambda \sin 2\theta} \qquad (81)$$

which is seen to be an inverse square function of the initial spin s_n^2.

B. Internal Forces

The next question of interest is with regard to the forces which cause the internal bending, sloshing, etc. Initially, each element of mass dm in the body has impressed upon it a large centrifugal acceleration $\dot{\psi}^2 \rho$ (see Fig. 31) which gradually damps out. The fluctuations arise out of the coupling of $\dot{\psi}$ with $\dot{\phi}$, the precession rate. For this portion of the analysis a new coordinate system is defined, also based on conventional Euler angles.

Let an orthogonal triple ζ, η, z be defined along the body-fixed roll axis, the origin being $\bar{z}$ above the inertial

---

[12]Or as an input, β, from Section IV, which is the final wobble angle at the end of the thrusting phase.

Fig. 31. Rotating coordinate system

origin The ζ axis is constrained to pass through the Z_0 axis at all times. Hence, the new axis rotates about the inertial X_0-Y_0-Z_0 axes at a rate $\dot{\phi}$. The dista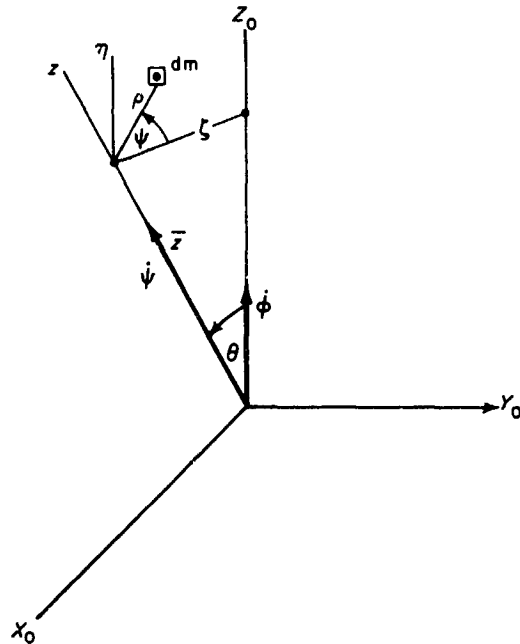nce $\bar{z}$ defines the distance along z where the element of mass dm is situated. The fact that $\dot{\theta} \neq 0$ will be neglected here, since the rate of change of wobble angle is normally orders of magnitude less than $\dot{\phi}$ and $\dot{\psi}$. It is also seen that the discussion of the forces on dm will be independent of ϕ, hence ϕ may be explicitly omitted, since the coordinate system will be defined when $\phi = 0$.

The problem may then be stated as: given a coordinate system (ζ, η, z) rotating about an inertial system $(X_0$-Y_0-$Z_0)$ at an angular rate $\dot{\phi}$ which will be time variable. A particle dm at a distance ρ from the z axis is rotating in the ζ, η, z system at a rate $\dot{\psi}$. What are the nonconstant forces on dm?

Since ρ and $\bar{z}$ are constant with time, in the general equation for the acceleration of a point in a rotating reference frame (see, for example, Ref. 11, p. 210), all but the centrifugal and coriolis terms vanish. The mass dm is seen to have a centrifugal acceleration $\rho \dot{\psi}^2$ with respect to the moving z-axis; and as seen in Fig. 31, an acceleration $\dot{\phi}^2 (\bar{z} \sin \theta - \rho \cos \theta \cos \psi)$ with respect to the Z_0-axis. Since the fluctuating terms are of principal concern, one pertinent force parallel to the X_0-Y_0 plane plane is

$$F_1 = -\dot{\phi}^2 \rho \cos \theta \cos \psi \, dm \qquad (82)$$

The coriolis term in the general acceleration equation is $2 \, \omega \times v$, where ω is the $\dot{\phi}$ vector as reflected in the ζ, η, z axes.

$$\omega = \dot{\phi} \sin \theta \, \boldsymbol{i} + \dot{\phi} \cos \theta \, \boldsymbol{k}$$

where the unit triple $\boldsymbol{i}, \boldsymbol{j}, \boldsymbol{k}$ is defined in the ζ, η, z frame. The velocity of dm in the ζ, η, z frame is

$$v = \rho \dot{\psi} \sin \psi \, \boldsymbol{i} + \rho \dot{\psi} \cos \psi \, \boldsymbol{j}$$

and the coriolis acceleration is then

$$2(\omega \times v) = 2(-\rho \dot{\psi} \dot{\phi} \cos \theta \cos \psi \, \boldsymbol{i} + \rho \dot{\psi} \dot{\phi} \cos \theta \sin \psi \, \boldsymbol{j}$$
$$+ \rho \dot{\psi} \dot{\phi} \sin \theta \cos \psi \, \boldsymbol{k}$$

The magnitude of this in the ζ-η plane is seen to be constant, $\rho \dot{\psi} \dot{\phi} \cos \theta$ rotating at a frequency $\dot{\psi}$. Thus, an observer sitting in dm would not experience a fluctuating force in this plane. The fluctuating force is along the z-axis and is

$$F_z = 2 \rho \dot{\psi} \dot{\phi} \sin \theta \cos \psi \, dm \qquad (83)$$

F_1 and F_2 can be vectorially added to determine that the component of force normal to the ζ-η plane (i.e., along the z-axis) is

$$F_z = (2\dot{\psi} \dot{\phi} - \dot{\phi}^2 \cos \theta) \rho \sin \theta \cos \psi \, dm \qquad (84)$$

and the component in the ζ-η plane is

$$F_{\zeta, \eta} = F_1 \cos \theta = -\dot{\phi}^2 \rho \cos \psi \cos^2 \theta \, dm \qquad (85)$$

However, the important thing to note is that the force in either plane can be expressed as

$$F = f(\rho, \dot{\phi}, \dot{\psi}, \theta) \cos \psi \, dm$$

C. Variation of $\dot{\phi}$ and $\dot{\psi}$ with θ

As θ increases due to the internal dissipation of energy and the body seeks a higher inertia, spin is transferred from $\dot{\psi}$ to $\dot{\phi}$ in such a way as to conserve the angular momentum. The relation between these two is found from

$$J_z = I_z \omega_z = J_0 \cos \theta$$

and $\quad J_0 = I_z s_0 \quad$ where s_0 is the design spin rate, ideally all about the z-axis, and

$$\omega_z = \dot{\phi} \cos \theta + \dot{\psi}$$

From the first two equations above, $\omega_z = f(\theta)$ is determined where substitution in the third yields

$$\dot{\psi} = (s_0 - \dot{\phi}) \cos \theta \qquad (86)$$

Thus, it is seen that when $\theta = 0$, $\dot{\psi} + \dot{\phi} = s_0$. The dependence of $\dot{\phi}$ upon θ is seen from

$$J_x^2 + J_y^2 = I_x^2 (\omega_x^2 + \omega_y^2) = J_0^2 \sin^2 \theta$$

$$\begin{cases} \omega_x = \dot{\phi} \sin \theta \sin \psi + \dot{\theta} \cos \psi \\ \omega_y = \dot{\phi} \sin \theta \cos \psi - \dot{\theta} \sin \psi \end{cases}$$

whence it may be determined that

$$\dot{\phi}^2 = s_0^2 (\lambda + 1)^2 - \dot{\theta}^2 \csc^2 \theta \qquad (87)$$

Here it is seen that if $\dot{\theta}$ is assumed zero, then $\dot{\phi}$ is constant and the device for transferring the spin from $\dot{\psi}$ and $\dot{\phi}$ is no longer real. When $0 < \theta \leq 90$ deg, $\dot{\phi}$ is well defined, and as $\theta \rightarrow 90$ deg, the right hand term becomes $\dot{\theta}^2 \csc^2 \theta \rightarrow \dot{\theta}^2$ and

$$\dot{\phi}^2 = s_0^2 (\lambda + 1)^2 - \dot{\theta}^2 \qquad (88)$$

for a final value. As $\theta \to 0$, the $\dot{\phi}$ and $\dot{\psi}$ tend toward coincidence, and the orthogonal system loses one degree of freedom and the solution of Eq. (50) has as a root $\sin \theta = 0$. Since at $\theta = 0$, $\omega_x = \dot{\phi} + \dot{\psi}$, the degree of freedom may be used by stating that $\dot{\phi} = 0$. This assumption is apparent since in Eq. (82), F_1 must vanish when $\theta = 0$ (all acceleration is constant), thus $\dot{\phi} = 0$. In the same manner, F_2 vanishes at $\theta = 0$; when $\theta = 90$ deg, all acceleration is along the z-axis, hence $F_1 = 0$; and since $\dot{\psi} = 0$ (Eq. 86), $F_2 = 0$.

Defining $\dot{\phi} = 0$ when $\theta = 0$ and $\dot{\phi} = s_0^2 (\lambda + 1)^2 - \dot{\theta}^2 \csc^2 \theta$, the moment $\phi > 0$ might seem inconsistent. However, the coupling between $\dot{\phi}$ and $\dot{\psi}$ (through θ) is perfectly valid when $\theta > 0$. In fact, Eq. (87) is exact. It is at the singularity $\theta = 0$ that difficulties arise. Since $\dot{\phi}$ and $\dot{\psi}$ are indistinguishable then (with respect to the mathematical interpretation, but not to the physical), $\dot{\phi}$ may arbitrarily be picked.

The forces on the element dm are then seen from Eqs. (84) and (85) to be (assuming $\dot{\theta} = 0$ in Eq. (87)

$$F_z = - s_0^2 (1 + \lambda) \rho \sin \theta \cos \theta \cos \psi \, dm$$

$$F_{\zeta\eta} = - s_0^2 (1 + \lambda)^2 \rho \cos^2 \theta \cos \psi \, dm \qquad (89)$$

The value of $\dot{\theta}$ to be used in determining $\dot{\phi}$ (Eq. 87) is that in Eq. (76), which in turn needs dT/dt as an input; hence, an iterative solution is required. If, at the end of spin-up, injection, etc., s_0 and θ_0 are known, then $\dot{\phi}_0$ can be determined from Eq. (51). F_1 and F_2 for the first increment of time can be found. Then from experimental damping data, energy dissipation is determined, i.e., dT/dt. $\dot{\theta}$ is calculated from Eq. (76) and substituted into Eq. (87), where a new, larger value of $\dot{\phi}$ is found. The iterative loop is continued as $\theta \to 90$ deg.

D. Effect of Initial Spin on Tumble Rate[13]

Since the ratio of the kinetic energy T to T_0 is independent of initial spin (s_0) the motion of the same body (λ) can be compared at several different s_0. This is because the motion will always be of the form in Eq. (79), dependent only on λ and θ.

Let the motion of the element of mass dm be approximated by a linear oscillator, the equation of motion of which is[14]

$$dm \left(\ddot{u} + \frac{\omega_0}{Q} \dot{u} + \omega_0^2 u \right) = F_0 \cos \dot{\psi} t \qquad (90)$$

where ω_0 is the natural frequency of dm, u the displacement, and Q the ratio of total energy to energy dissipated in one period. F_0 is the magnitude of the fluctuating driving force discussed in Section B, and can be characterized as $F_0 = s_0^2 C_1 (\lambda, \theta)$, where C_1 is independent of s_0, and is only a function of the shape of the body and the wobble angle θ. The frequency $\dot{\psi}$ can be written as $s_0 C_2 (\lambda, \theta)$ from Eqs. (86) and (87) (letting $\dot{\theta} = 0$). The solution can then be written as

$$u = \frac{s_0^2 F_0 \cos (\dot{\psi} t + \delta)}{\sqrt{(\omega_0^2 - C_2^2 s_0^2)^2 + (\omega_0 C_2 s_0 / Q)^2}} \qquad (91)$$

where

$$\delta = \tan^{-1} - \frac{\omega_0 C_2 s_0}{Q (\omega_0^2 - C_2^2 s_0^2)}$$

Note here that the time varying value of F_0 was integrated as though it were a constant. This is allowable for two reasons: first, s_0 is usually orders of magnitude greater than $\dot{\theta}$, the driving force behind F_0; and second, an attempt is being made to determine the effect of varying s_0 on identical bodies (i.e., λ's are equal). This implies that the way in which the body varies its internal energy is determined by Eq. (79), which is a function of θ alone once λ is stipulated. Hence, for comparison purposes, it little matters what form F_0 assumes.

The energy dissipation is obtained from the energy integral when nonconservative forces are involved and is

$$\frac{dT}{dt} = \mathcal{F}_1 \dot{u} \qquad (92)$$

where $\mathcal{F}_1$ is the nonconservative force, which, in this case, is the damping term,

$$\mathcal{F}_1 = \frac{\omega_0}{Q} \dot{u} \, dm \qquad (93)$$

whence

$$\frac{dT}{dt} = \frac{\omega_0}{Q} \dot{u}^2 \, dm$$

---

[13]This Section is an expansion of a private communication from Professor Leverett Davis, Jr., of California Institute of Technology to the author.

[14]The equations and analysis here can for the most part be found in the first two chapters of Ref. 10.

u is calculated from Eq. (91). Since $\dot{u}^2$ is an oscillating function $[\sin^2(\dot{\psi}t + \delta)]$, the average value of $\dot{T}$ over one cycle is

$$\left\langle \frac{dT}{dt} \right\rangle_{AV} = \frac{\omega_0}{Q} \left\langle \dot{u}^2 \right\rangle_{AV} dm$$

$$= \frac{s_0^6 \, C_2^2 \, F_0^2}{\left(\omega_0^2 - C_2^2 \, s_0^2\right)^2 + \left(\frac{\omega_0 C_2 s_0}{Q}\right)^2} \cdot \frac{\omega_0}{2Q} dm$$

(94)

The equation for θ is then

$$\frac{d\theta}{dt} = \left[\frac{C_2^2 \, F_0^2}{2 \, I_z \, \lambda \sin 2\theta} \right] \left[\frac{\frac{1}{Q} \, \omega_0 \, s_0^4}{\left(\omega_0^2 - C_2^2 \, s_0^2\right)^2 + \left(\frac{\omega_0 C_2 s_0}{Q}\right)^2} \right]$$

(95)

Three cases present themselves:

a. If the natural frequency is very high (rigid system), so that $\omega_0 >> s_0$, and the damping is very small, $Q >> 1$, which implies $\omega_0 >> s_0/Q$, then Eq. (95) reduces to

$$\dot{\theta}_a = P \frac{s_0^4}{Q \omega_0^3}$$

where

$$P = \frac{C_2^2 \, F_0^2}{2 \, I_z \, \lambda \sin 2\theta},$$

and the rate of change of θ is proportional to s_0^4. Hence, the time required to go the same number of degrees (say from 2 to 75) would be proportional to $1/s_0^4$.

b. If Q is very small (large damping), so that $s_0/Q >> \omega_0 >> s_0$, then Eq. (95) becomes

$$\dot{\theta}_b = P \frac{Q \, s_0^2}{\omega_0 C_2^2}$$

and the time to go between equal values of θ is proportional to $1/s_0^2$.

c. When the natural frequency of the system is low, i.e., $s_0 >> \omega_0$, then

$$\dot{\theta}_c = P \frac{\omega_0}{Q \, C_2^4}$$

and $\dot{\theta}$ (and time) is independent of s_0.

If $\dot{\psi}$ passes through a resonant frequency, $\dot{\psi} = \omega_0$ at some point of the transition, then the energy dissipation will be greater. The magnitude of θ is also a strong function of ω_0 and Q. In case a, where $\omega_0 >> s_0 >> s_0/Q$, then $\dot{\theta}_a < P$. In case b, where Q is small, and ω_0 and s_0 are intermediate, it may be approximated that $\dot{\theta}_b \approx P$ ($C_2^2 < 1$). In case c, where ω_0 is small and Q is intermediate, $C_2^4 << 1$, and it follows that $\dot{\theta}_c > P$. It may be generalized that

$$\dot{\theta}_c > \dot{\theta}_b > \dot{\theta}_a$$

Explorer I, with its long whip antennae with low natural frequency, fell in case c.

As a rough cut of the time required to tumble, if $\langle dT/dt \rangle$ is assumed constant over the range of interest, then

$$\Delta t = \frac{T_{max} - T_{min}}{\langle dT/dt \rangle_{av}} = \frac{1}{2} \, s_0^2 \, (I_x - I_z) \left\langle \frac{dT}{dt} \right\rangle_{AV}^{-1}$$

where $\langle dT/dt \rangle_{AV}^{-1}$ is determined from Eq. (94).

E. Discussion

The problem may be reduced to this: Since the dynamical relations (Section V-A) and forces on the element (Section V-B) are known, it remains only to (1) recognize those elements of the body which will be affected by the forces, (2) define the mathematical model to which each belongs, and (3) determine the values of the constants to be used.

General conclusions are best summed up by describing items to be avoided when designing bodies for spin.

1. Try to make roll inertia greater than the inertia in other axes (e.g., Apollo), in which case the problem vanishes.

2. If this cannot be accomplished, make the body as rigid as possible, avoiding any liquids, dangling wires, etc. Make all bulkheads parallel to the roll axis stiff.

3. If neither 1 nor 2 is possible, keep the design spin rate s_0 as small as possible within other system constraints.

In general, it appears from past results that this phenomenon is not hard to design around. If, by merely removing the whip antennae on an *Explorer I*, the tumble rate was decreased by over two orders of magnitude, then one may conclude that internal damping is something one designs in rather than out of the typical spinning body.

VI. SUMMARY AND GENERAL CONCLUSIONS

A. Error Plan Summary

The overall errors discussed in the Report are depicted in Fig. 32, and can be somewhat broken down into chronological order.

Section III

a. Initial errors of spin-up. These are two: a tip-off angular velocity $\dot{\theta}_0$, and an error angle at time of spin-up which is $\Theta_0 + \dot{\theta}_0 \delta t$, Θ_0 being the initial displacement, δt being the time from release to initiation of spin-up.

b. Dispersion of the angular momentum vector from the inertial axes during spin-up (a_i).

c. The wobble angle produced during spin-up (β).

Section IV

a. Velocity vector dispersion angle (α) produced by the initial conditions and the misalignment of the thrust vector.
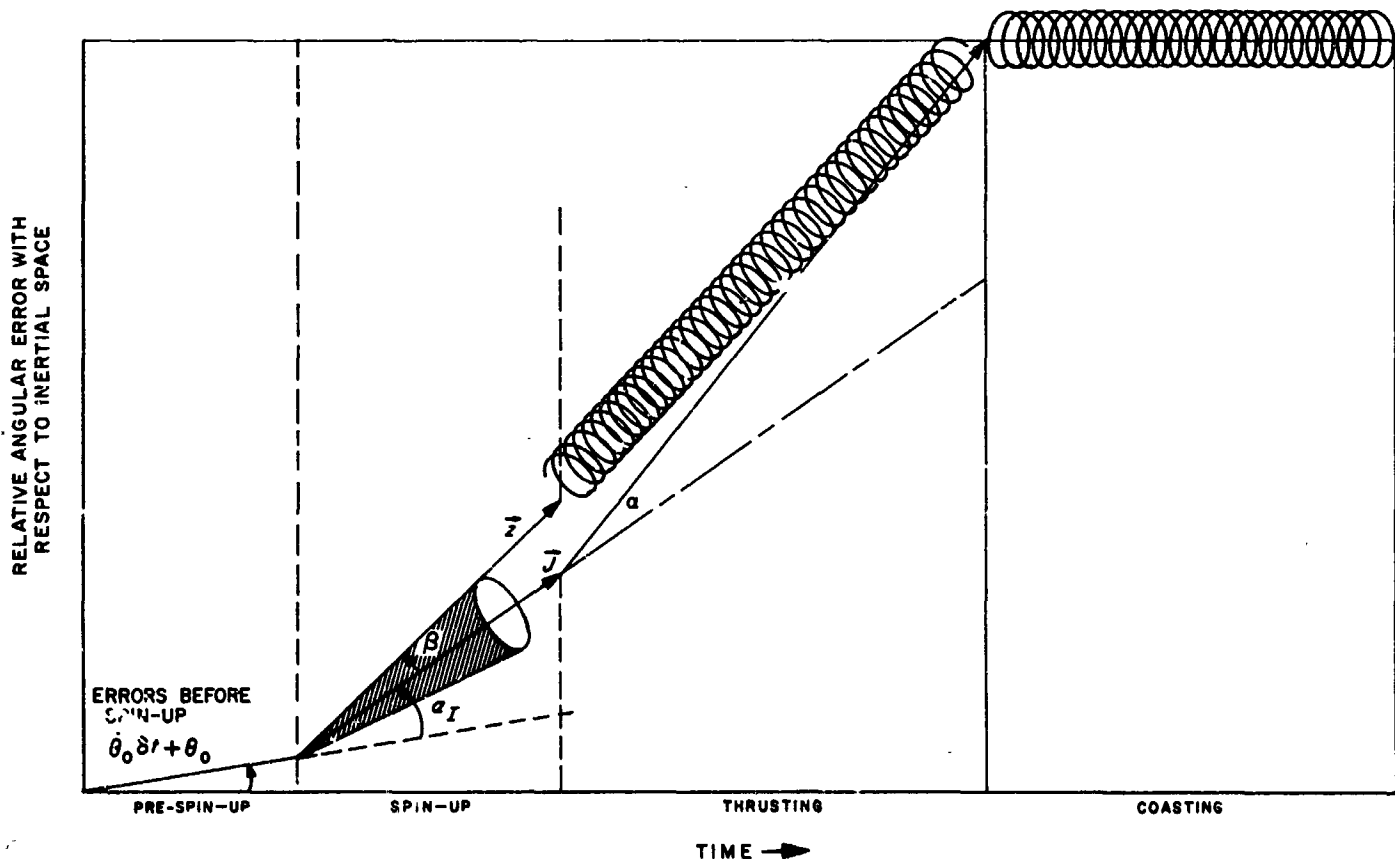

Fig. 32. Overall error plan

b. Velocity vector dispersion magnitude.

c. Final wobble angle (β_1).

Section V

a. Effects of nonrigidity on wobble angle. This part is not an error (as in Sections III and IV), however it can affect the spacecraft performance if neglected.

B. General Conclusions

The first two conclusions may be stated categorically, (1) whenever possible, $\lambda > 0$, i.e., the inertia about the spin axis should be as great as possible. If this is true,

errors in Sections III and IV are minimized with respect to shape, and the discussion in Section V does not apply; and (2) all error sources, such as initial conditions, thrust misalignment, etc., should be minimized. Other conclusions are: (3) during spin-up, both the spin torque and the spin rate should be as large as possible; (4) when thrusting, the number of revolutions through which the body turns should be as high as possible, i.e., $s_0 t_b$ should be large. As a rule of thumb (noted from the results of Section IV), if $s_0 t_b / 2\pi < 3$ revolutions, then little is gained by spinning; and (5) for coast stability, the body should be as rigid as possible and be spinning at the lowest possible spin rate. The obvious contradiction between conclusions 4 and 5 is resolved by despinning after thrusting. Appendix E contains general equations for despinning by the "yo-yo" method.

REFERENCES

1. Leon, H. I., *Spin Dynamics of Rockets and Space Vehicles in Vacuum*, Space Technology Laboratory TR-59-0000-00787, September 16, 1959.

2. Goldstein, H., "Classical Mechanics," Addison-Wesley, Reading, Massachusetts, 1959.

3. Jahnke-Emde-Losch, "Tables of Higher Functions," McGraw-Hill Book Co. Inc., New York, N. Y., 1960.

4. Davis, L., Jr., Follin, J. W., Jr., and Blitzer, L., "Exterior Ballistics of Rockets," D. Van Nostrand Co., Inc., Princeton, New Jersey, 1958.

5. Pearcy, T., "Table of the Fresnel Integral to Six Decimal Places," Cambridge University Press, 1956.

6. Syrett, H. E., and Wilson, M. W., "Computation of Fresnel Integrals to 28 Figures: Approximation to 8 and 20 Figures," Computer Science Department, University of Western Ontario, London, Ontario.

7. Rosser, J. B., *Theory and Application of* $\int_0^z e^{-x^2} dx$ *and* $\int_0^z e^{-p^2y} dy \int_0^y e^{-x^2} dx$ *Part I, Methods of Computation*, Final Report B2.1 from Allegany Ballistics Laboratory, OSRD 5861.

8. Rosser, J. B., Newton, R. R., and Gross, G. L., "Mathematical Theory of Rocket Flight," McGraw-Hill Book Co. Inc., New York, N. Y., 1947.

9. Pilkington, W. C., *Vehicle Motions as Inferred from Radio-Signal-Strength Records*, External Publication No. 551, Jet Propulsion Laboratory, Pasadena, California, September 5, 1958.

10. Slater, J. C. and Frank, N. H., "Mechanics," McGraw-Hill Book Co. Inc., New York, N. Y., 1947.

11. Lass, H., "Vector and Tensor Analysis," McGraw-Hill Book Co. Inc., New York, N. Y., 1950.

12. Powell, R. B. and Smith, R. L., *Dynamics of Spinning Re-entry Bodies*, AIAA Paper No. 64-470, June 1964.

13. Wilson, R. H., Jr., *Rotational Magnetodynamics and Steering of Space Vehicles*, NASA TN-D566, September 1961.

14. Creech, M. D. and Fergin, R. K., "The Yo-Yo De-spinners . . . New Mechanism Stops Spin of Rotating Masses," *Product Engineering*, p. 597, April 3, 1961.

15. Cornille, H. J., Jr., *A Method of Accurately Reducing the Spin Rate of a Rotating Spacecraft*, NASA TN D-1420, October 1962.

16. Fedor, J. V., *Theory and Design Curves for a Yo-Yo De-Spin Mechanism for Satellites*, NASA TN D-708, August 1961.

17. Fedor, J. V., *Analytical Theory of the Stretch Yo-Yo for De-Spin of Satellites*, NASA TN D-1676, April 1963.

APPENDIX A

Orthogonal Transformation for Analog Simulation

If an analog simulation of spinning dynamics is desired (including the angular rate transformation from body-fixed to inertial coordinates), the conventional Euler angles defined in Section II are found to be unsatisfactory. This can be seen from Eq. (50), which gives the angular rate transformation

$$\begin{bmatrix} \omega_x \\ \omega_y \\ \omega_z \end{bmatrix} = \begin{bmatrix} \sin\theta\sin\psi & \cos\psi & 0 \\ \sin\theta\cos\psi & -\sin\psi & 0 \\ \cos\theta & 0 & 1 \end{bmatrix} \begin{bmatrix} \dot\phi \\ \dot\theta \\ \dot\psi \end{bmatrix}$$

For the solution, the inverse of the above equation is required, or, if the matrix is Λ,

$$\begin{bmatrix} \dot\phi \\ \dot\theta \\ \dot\psi \end{bmatrix} = \frac{1}{|\Lambda|} \| \Lambda \| \begin{bmatrix} \omega_x \\ \omega_y \\ \omega_z \end{bmatrix} \qquad (A\text{-}1)$$

where $|\Lambda|$ is the determinant of Λ and $\|\Lambda\|$ is the adjoint of Λ. By inspection, $|\Lambda| = -\sin\theta$, and since θ is nominally zero, or if not, almost zero, the equations in (A-1) are unstable for analog simulation. Another set of Euler angles must be defined in which the determinant of the angular rate matrix is not nominally zero. Figure A-1 shows one possible transformation which is stable over the region of interest. The rotations, in order, are

$$[A] = \begin{bmatrix} 1 & 0 & 0 \\ 0 & \cos A & \sin A \\ 0 & -\sin A & \cos A \end{bmatrix}$$

$$[G] = \begin{bmatrix} \cos G & \sin G & 0 \\ -\sin G & \cos G & 0 \\ 0 & 0 & 1 \end{bmatrix}$$

$$[\theta] = \begin{bmatrix} \cos\theta & 0 & -\sin\theta \\ 0 & 1 & 0 \\ \sin\theta & 0 & \cos\theta \end{bmatrix}$$
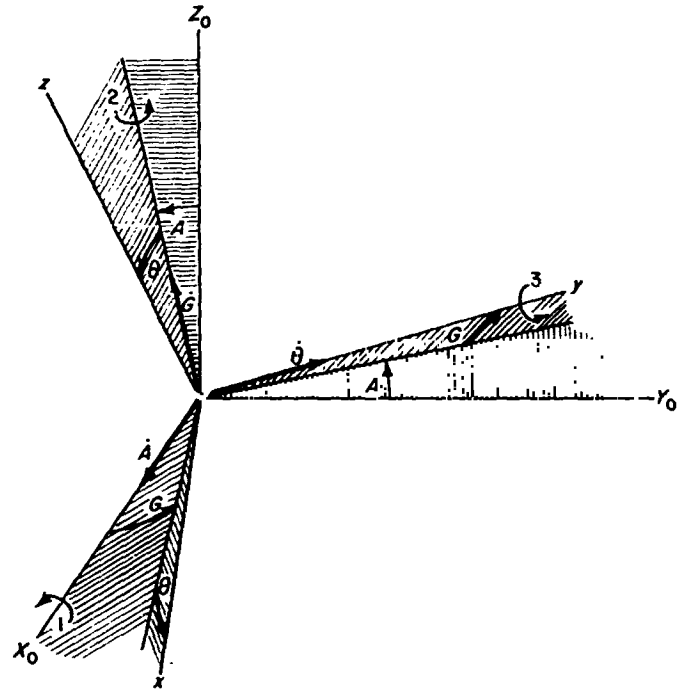

Fig. A-1. Orthogonal transformation

and the angular rate transformation is

$$\begin{bmatrix} \omega_x \\ \omega_y \\ \omega_z \end{bmatrix} = \begin{bmatrix} \cos G \cos\theta & -\sin\theta & 0 \\ -\sin G & 0 & 1 \\ \cos G \sin\theta & \cos\theta & 0 \end{bmatrix} \begin{bmatrix} \dot A \\ \dot G \\ \dot\theta \end{bmatrix}$$

$$(A\text{-}2)$$

which can be verified from Fig. A-1. The determinant of the matrix in Eq. (A-2) is $-\cos G$, which if the body-fixed y-axis is defined as that of spin, is nominally unity. Hence, stable solutions of the inverse of Eq. (A-2) result. The fully expanded transformation of the three rotations is

$$[\theta][G][A] = \begin{bmatrix} \cos G \cos\theta & \sin G \cos A & -\cos G \sin\theta + \sin G \sin A \cos\theta \\ -\sin G \cos\theta + \cos G \sin A \sin\theta & \cos G \cos A & \sin G \sin\theta + \cos G \sin A \cos\theta \\ \cos A \sin\theta & -\sin A & \cos A \cos\theta \end{bmatrix}$$

whence any body-fixed vector v is transformed into an inertial vector V_0 by

$$V_0 = [A]^{-1} \cdot [G]^{-1} \cdot [\theta]^{-1} v$$

APPENDIX B

Exact Formulation and Numerical Solution

I. NONLINEAR EFFECTS

If nonlinearities are present in the system, the basic differential Eq. (41) and subsequent equations cannot be explicitly solved. These nonlinearities usually arise out of more exact formulations of the problem.

a. Variable Mass During Burning. The largest single cause of inaccuracies in Section IV is the mass decrease during burning, which decreases inertia. A good mass approximation assumes a constant thrust, thus constant mass flow rate,

$$m = m_0 - \dot{m}\,t = m_0 - \left(\frac{F}{I_{SP}}\right)t \qquad \text{(B-1)}$$

where m_0 is the total mass at $t = 0$, and I_{SP} is the rocket propellant specific impulse. Inertia changes may then be characterized. If the rocket motor is considered a point mass at the end of a thrusted body (see Fig. B-1), then the inertia change in the cross axes (pitch-yaw) is the initial inertia decreased by a changing mass effect as determined by the parallel axes theorem. In effect, the "rigid body" mass (M) remains constant, while the rocket motor attached to one end decreases in mass (m). The pitch inertia (as a function of time) is

$$I_x(t) = I_M + I_m + Mx^2 + m(l - x)^2 \qquad \text{(B-2)}$$

where I_M = inertia of M (rigid body) about its c.m.

I_m = inertia of m (rocket motor) about its c.m.

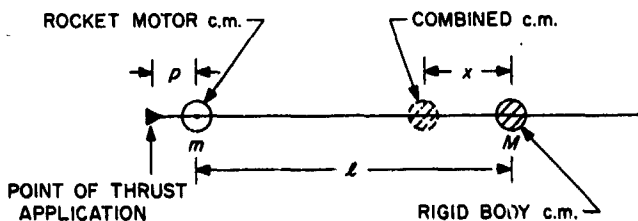l = distance between mass centers (can be

variable).

$$x = \frac{m}{M + m}\,l$$

ROCKET MOTOR c.m.

COMBINED c.m.

POINT OF THRUST APPLICATION

RIGID BODY c.m.

Fig. B-1. Schematic of mass variation

and $m(t)$ is given by Eq. (B-1). The torque about the pitch axis is then

$$L_r = F\,\zeta\,(p + l - x) \qquad \text{(B-3)}$$

If the assumption of $\dot{m}$ made in Eq. (B-1) is not valid, then whatever $m(t)$ is assumed must be pointwise integrated.

Decreases in the roll inertia can be neglected, since to a first order the mass thrown out by the motor takes with it angular momentum, keeping the spin rate about the roll axis constant at s_0. Except in cases of very large mass decreases during spinning, the variation of I_z can probably be neglected (since the mass of propellant being expelled is usually situated close to the roll axis, thus contributing only a small part of the total I_z. In the case for Apollo, all changes in inertia, both pitch and roll, are neglected. However, for *Ranger*, when ⅔ of its mass is expended during burning, these variations must be taken into account.

b. Jet Damping. When a body, rigid or not, has a cross-angular velocity (i.e., $\omega = \omega_x + i\omega_y \neq 0$) during the expulsion of mass along the z-axis, a damping arises out of the fact that the cross ω causes a "wagging" of the jet stream, i.e., a change in the direction of the linear momentum vector. The magnitude of this damping (Ref. 8, p. 21) is proportional to the rate of mass expulsion, and to the cross-angular rate. The damping occurs because, if ω increases, the rate of change of the linear momentum vector of the exhaust gases is greater, and thus causes a greater resistance to the increase in ω. If $\dot{m}$ is the mass flow rate, and the distance $(l + p - x)$ from the combined c.m. to the point of thrust application, the jet damping term is $-\omega\,\dot{m}\,(l + p - x)^2$.

c. Small Angle Approximations. The expediency of letting $\sin\theta \approx \theta$ and $\cos\theta \approx 1$ in the inertial transformation is obvious from the analysis. From practical considerations, this approximation is usually valid, since real systems seldom can tolerate angular disturbances greater than 5–10 deg without intolerable error buildup. If, however, this approximation cannot be used, the solutions of the inertial transformation must be made with the full Eulerian expansion, resulting in transcendental differential equations.

d. Roll Moment. During the burning of some rocket motors, a roll torque is generated. If this is to be considered, the ω_z vector in Eq. (41) is no longer constant, but must be varied according to the roll acceleration.

e. External Forces. Gravity and solar pressure are inertial forces, hence they may be neglected with respect to the spinning dynamics, but must be included in any velocity calculation (e.g., Eq. 62). Aerodynamic forces are only partially inertial since they depend on the angle of attack θ (sometimes on ϕ), and are independent of ψ in a body of revolution. Good discussions of aerodynamic forces can be found in Refs. 4 and 8.

f. Cross Products of Inertia. It has been assumed in this report that all cross-products vanish, since the present technology is such that the principle axes of the body and the geometrical axes can be made almost coincident in bodies of revolution. To consider the cross products,

the full inertia tensor must be included in Euler's dynamical equations and carried along in the subsequent analysis (see, for example, Ref. 1 or 12).

g. Nonrigid Effects. If the strain on structural members and mass deflections are to be considered, the problem increases tremendously. Euler's dynamical equations must be modified to include cross-products of inertia, time-varying coefficients, and other nonlinear effects discussed below. Each effect of nonrigidity must be treated separately, e.g., mass unbalance will affect inertia, cause cross-products, c.m. shift, etc.; straining of the structural members will cause mass unbalance, rotation of the thrust vector, etc.

h. General Nonlinear Effects. These include variations in thrust vector misalignment with time, variation of thrust with time, etc. Each one of these must be included in the basic differential equation and be numerically integrated.

II. GENERAL FORMULATION

Combining as many of the aforementioned effects as possible, the basic equation for the body-fixed ω is then

$$\dot{\omega} + i\,\omega_z(t)\left\{\lambda(t) - \dot{m}(l + p - x)^2\right\}\omega = \frac{L(t)}{I_z(t)} \quad \text{(B-4)}$$

where the time functions of ω_z, λ, x, l, L, I_z and $\dot{m}$ (if not constant) are to be stipulated. Equation (B-4) is then numerically integrated to determine the cross-angular

rates $\omega(t) = \omega_x(t) + i\,\omega_y(t)$, which, with the solution of $\omega_z = N_z(t)$ [if there is a torque in the z-direction] are substituted into Eq. (8). The numerical solution of this set of equations will give the time functions of the Euler angles (ϕ, θ, ψ) which define the inertial transformation matrix Γ. The inertial thrust vector is then determined, which, when divided by $m(t)$ and integrated, yields the inertial velocity vector.

III. SPECIFIC EXAMPLES

Ranger is an ideally suited example here, since ⅔ of the weight of the original system is expended. Table B-1 gives the parameters used in the problem.

Table B-1. *Ranger* parameters

Thrust F (constant), lb	5500
Burning time t_b, sec	9.6
Payload mass, lb	96.0
Flow rate $\dot{M}$ (constant), lb/sec	20.0
Spin rate s_0, rad/sec	30.0
Lever arm in (l) (variable), in.	See Fig. B-2
Pitch inertia I_z, lb-in.²	See Fig. B-2
Inertia ratio, λ	See Fig. B-2
Capsule mass, M, lb	See Fig. B-2
Thrust misalignment ζ, rad	0.004
Initial wobble angle θ_0, rad	0.001
$K = \dfrac{t_b F l}{\lambda I_z}$	See Fig. B-2

This problem is identical to that for *Ranger* in Section IV-J, except there, three points ($K = -5000, -10,000, -20,000$) were used to examine the effect of K on α. These three points are seen to represent the K vs t curve on Fig. B-2. Looking at Fig. B-3, the output of the above problem, it is seen that the $K = -10,000$ in the approximation is close to the true solution on Fig. B-3. However, the shape of the solutions do not agree too closely. If the proper value of K could be assumed, the approximate solution could suffice for values of $\alpha(t)$.

The Apollo problems in Section IV-J were also run on the big program to illustrate two points. If the mass change is small, the $\alpha(t)$ in Figs. 22–25 do in fact closely approximate the true solutions in Figs. B-4 through B-7. The other reason is that the larger program allows a look at V'_x vs V'_y and a_t real vs a_t imaginary. The Apollo problems were chosen because the high spin rate of the *Ranger* capsule made the curves too confusing. Figures B-8 through B-11 show V'_x vs V'_y for the problems listed in Section IV-J. The shape of the curves corroborates the statements made in Section IV-F. Figures B-12 through B-15 show a_t real vs a_t imaginary. This is the trace that a ray of light located along the body-fixed z-axis would make as seen by an observer sitting above the capsule in the inertial frame.
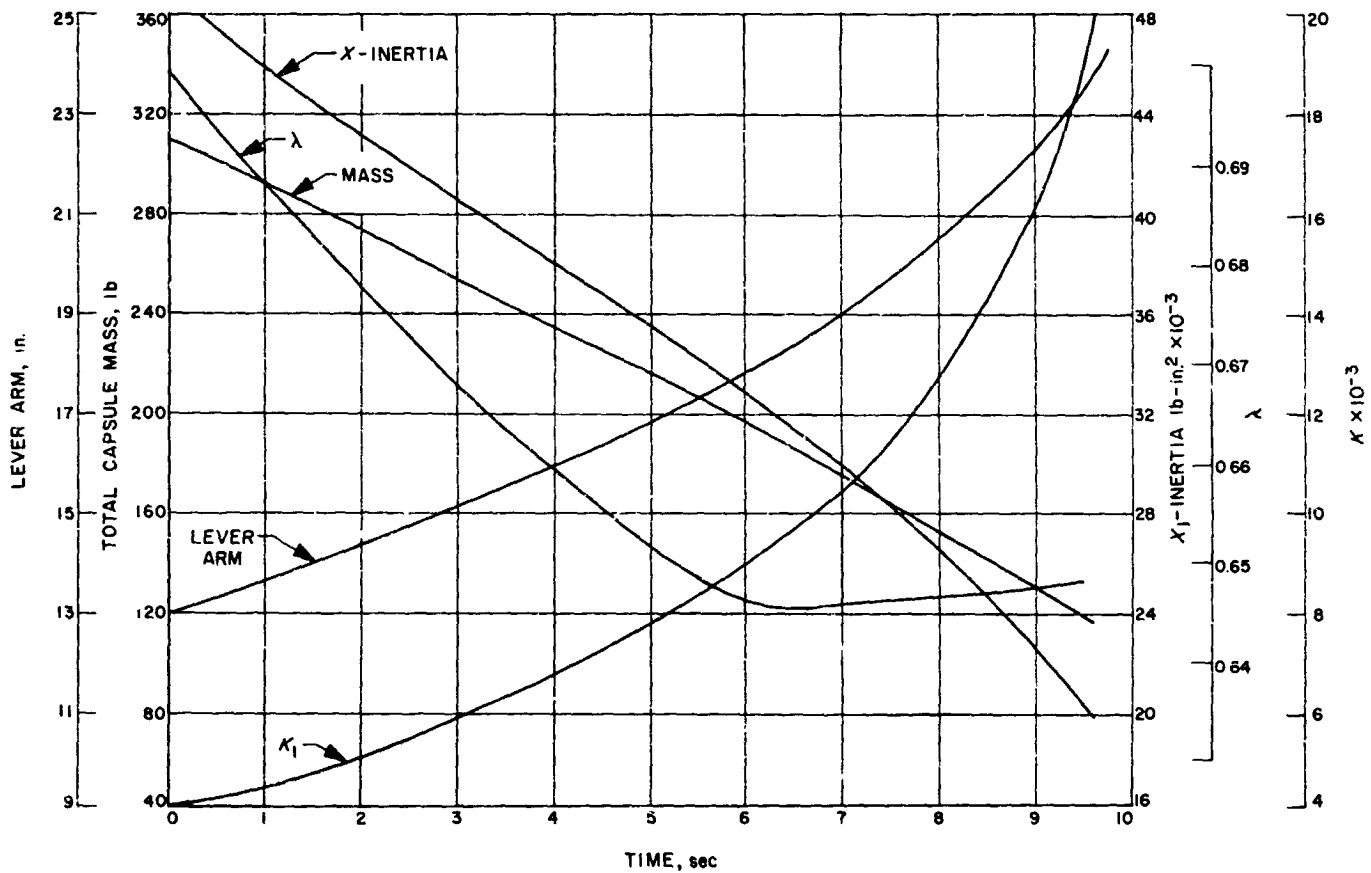
Fig. B-2. Plots of $\dot{m}$, I_z, K, λ and ℓ_j vs t_1 for Ranger capsule
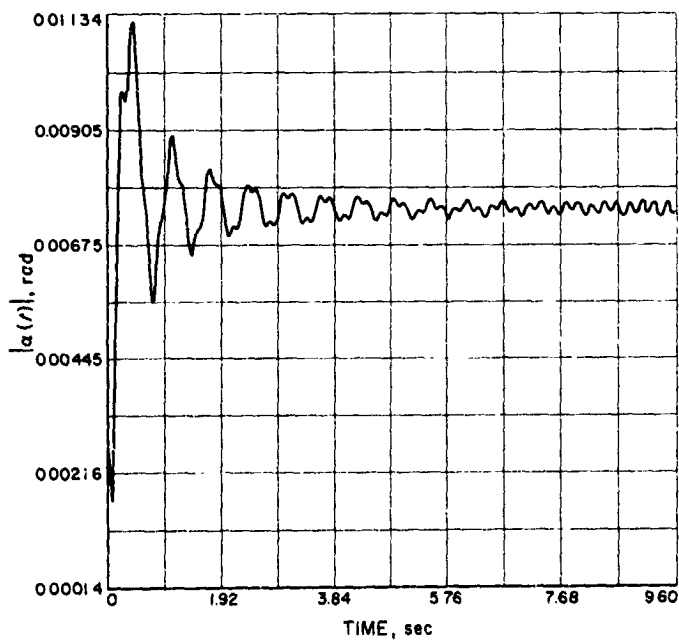
Fig. B-3. α (t) vs t for Ranger capsule (variable mass)
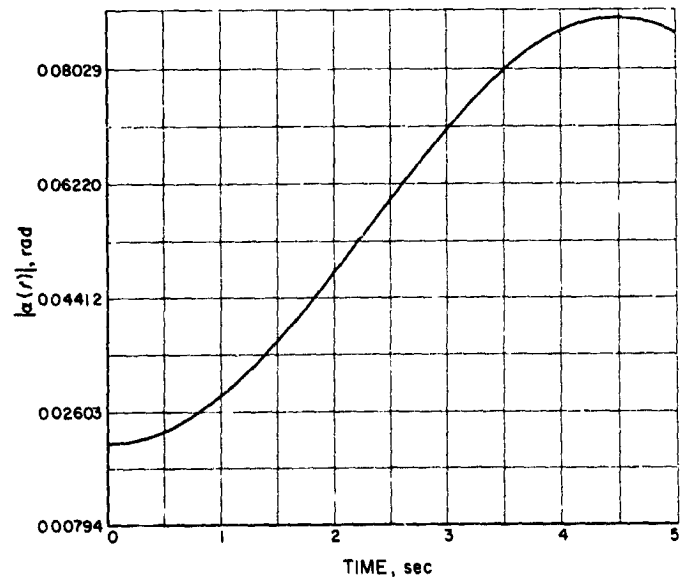
Fig. B-4. α (t) vs t for Apollo-shaped capsule (variable mass), $s_0 = 1$ rad/sec, $\theta_0 = 0.025$ rad
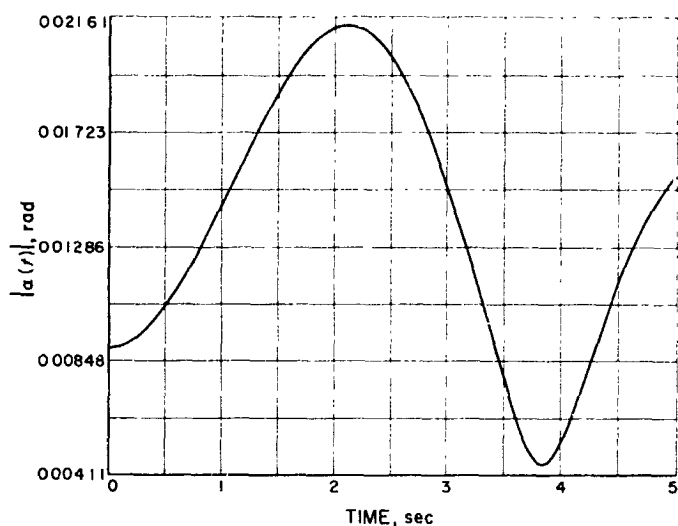
Fig. B-5. $\alpha(t)$ vs t for Apollo-shaped capsule (variable mass), $s_0 = 2$ rad/sec, $\theta_0 = 0.013$ rad
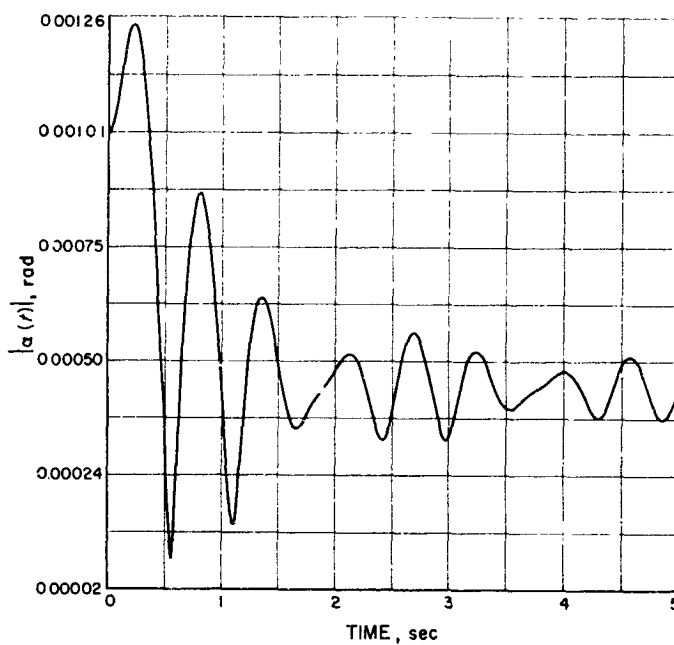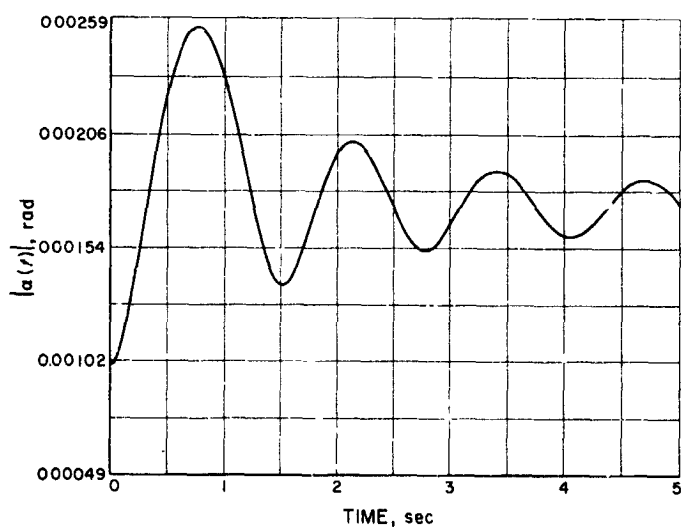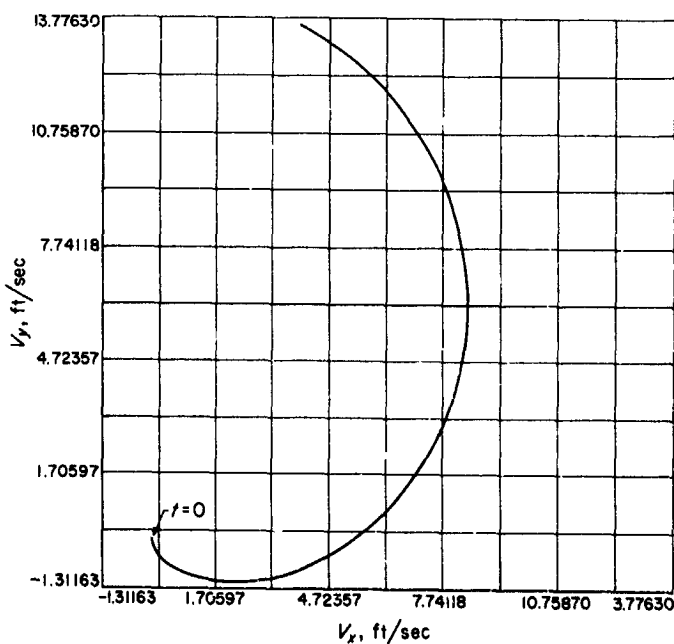

Fig. B-7. $\alpha(t)$ vs t for Apollo-shaped capsule (variable mass), $s_0 = 10$ rad/sec, $\theta_0 = 0.003$ rad

Fig. B-6. $\alpha(t)$ vs t for Apollo-shaped capsule (variable mass), $s_0 = 5$ rad/sec, $\theta_0 = 0.005$ rad

Fig. B-8. V_x vs V_y for Apollo-shaped capsule, $s_0 = 1$ rad/sec, $\theta_0 = 0.025$ rad
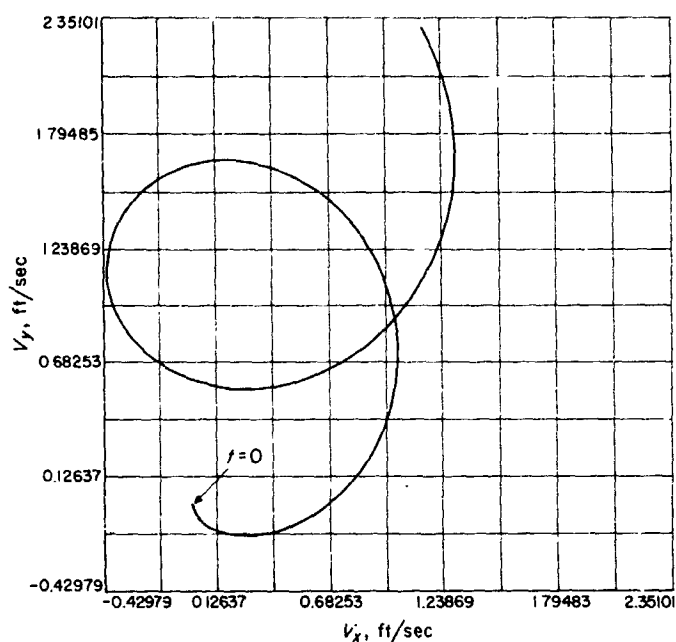
Fig. B-9. V_x vs V_y for Apollo-shaped capsule, $s_0 = 2$ rad/sec, $\theta_0 = 0.013$ rad
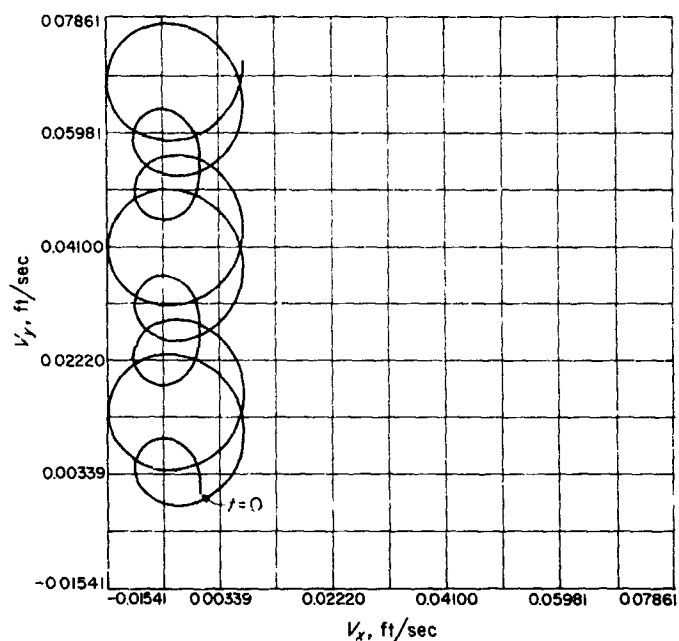

Fig. B-10. V_x vs V_y for Apollo-shaped capsule, $s_0 = 5$ rad/sec, $\theta_0 = 0.005$ rad

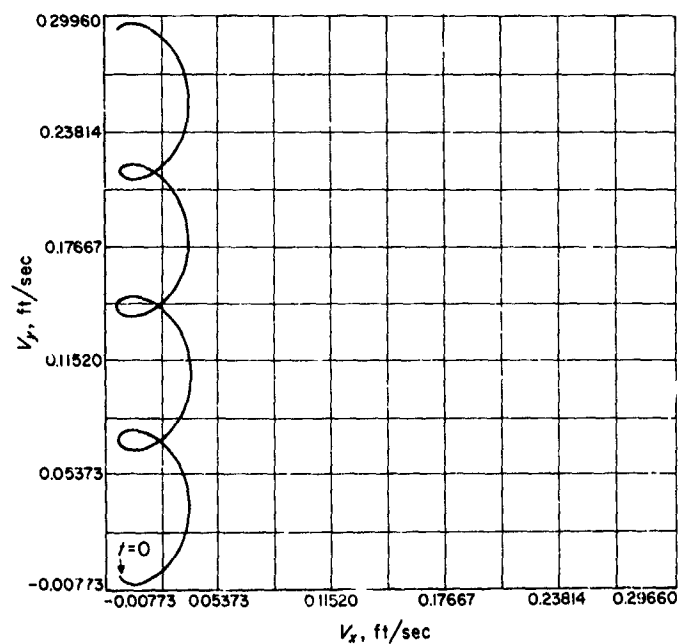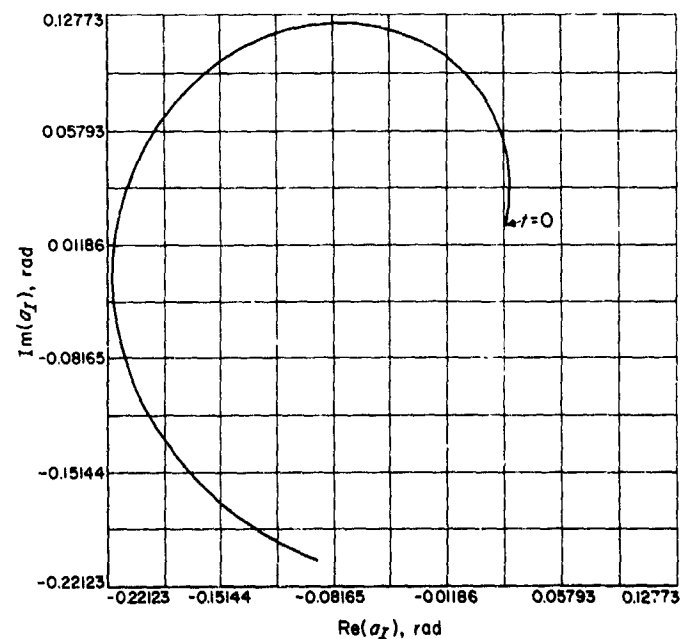Fig. B-11. V_x vs V_y for Apollo-shaped capsule, $s_0 = 10$ rad/sec, $\theta_0 = 0.003$ rad

Fig. B-12. $\mathcal{R}e\ a_I$ vs $\mathcal{J}m\ a_I$ for Apollo-shaped capsule, $s_0 = 1$ rad/sec, $\theta_0 = 0.025$ rad

Fig. B-13. $\mathcal{R}e\ a_I$ vs $\mathcal{I}m\ a_I$ for Apollo-shaped capsule, $s_0 = 2$ rad/sec, $\theta_0 = 0.013$ rad
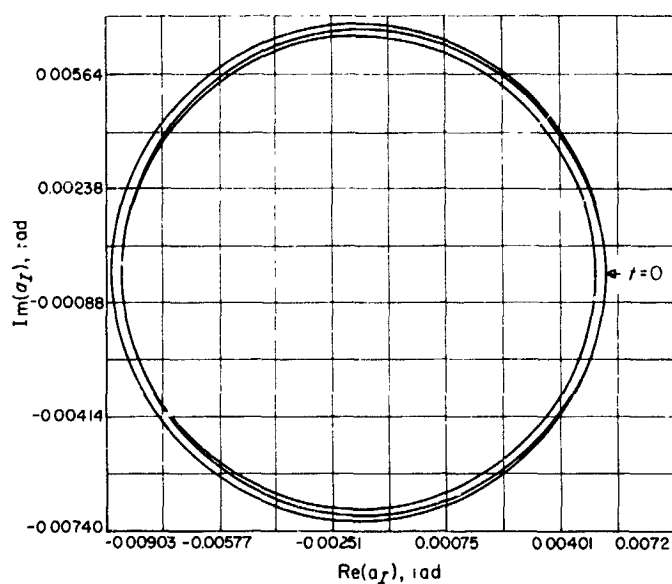
Fig. B-14. $\mathcal{R}e\ a_I$ vs $\mathcal{I}m\ a_I$ for Apollo-shaped capsule, $s_0 = 5$ rad/sec, $\theta_0 = 0.005$ rad

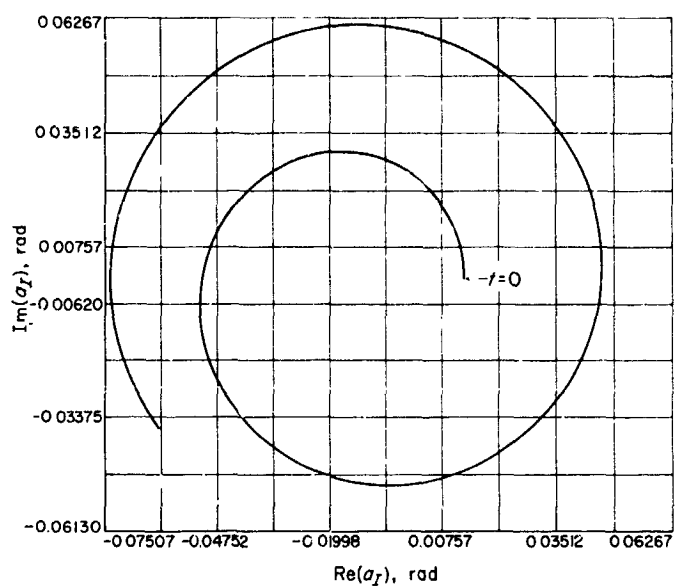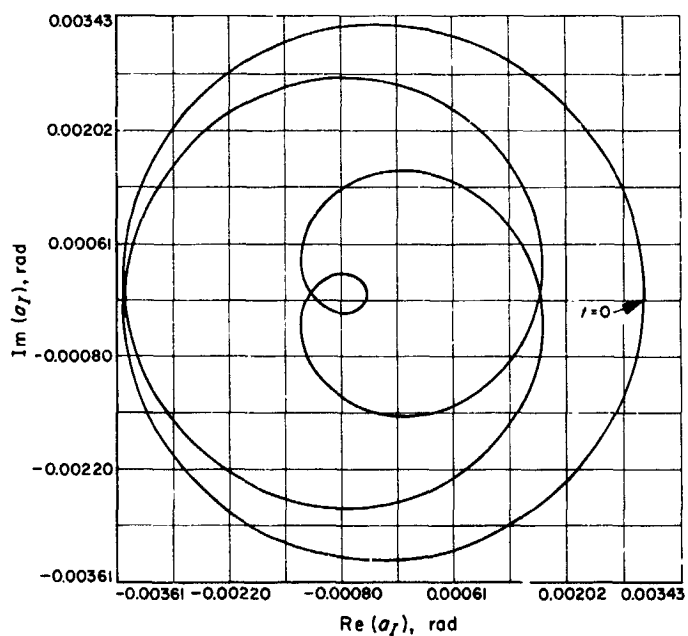**Fig. B-15.** $\mathcal{R}e\ a_I$ vs $\mathcal{I}m\ a_I$ for Apollo-shaped capsule, $s_0 = 10$ rad/sec, $\theta_0 = 0.003$ rad

APPENDIX C

Thrust Misalignment of Solid Propellant Rockets

An attempt is made in this appendix to justify the use of $\zeta = 0.004$ rad for effective thrust misalignment from data gathered from the in-flight measurements of the second and third stages of the Scout launch vehicle. All four stages of the Scout are solid propellant rockets; however, the first stage burns in the atmosphere, making any misalignment data almost impossible to separate from the aerodynamic effects, and the fourth stage is spin-stabilized. The middle two stages are attitude stabilized by bang-bang peroxide jets in pitch/yaw/roll.* Vehicle pitch and yaw motion and rates are telemetered and recorded. The slope of the pitch rate trace when the H_2O_2 jets are off gives the vehicle acceleration in the pitch plane; yaw acceleration is obtained in a like manner. The vehicle nominal thrust, inertia, mass, etc., is known as a function of flight time. Hence, the effective thrust misalignment may be determined in either the pitch or the yaw plane.** Figures C-1 and C-2 illustrate how the thrust misalignment varied on Scout flight S-127. Table C-1 lists maximum thrust misalignment in degrees for the second and third stages for 12 flights, ζ_p being the

---

*Roll deadband is $\approx \pm 1\frac{1}{2}$ deg. minimizing pitch/yaw coupling.

**This thrust misalignment is effective because it is what the vehicle sees from a torquing standpoint, hence it includes the effect of center-of-mass variations, vehicle bending, etc. It is therefore erroneous to speak of ζ as only a solid rocket thrust misalignment.
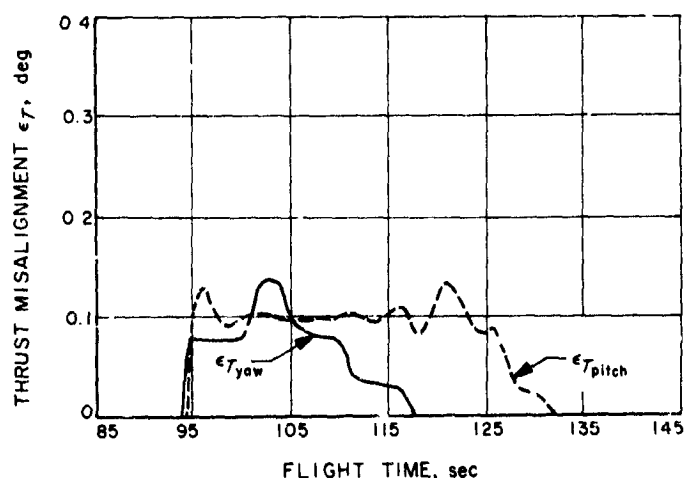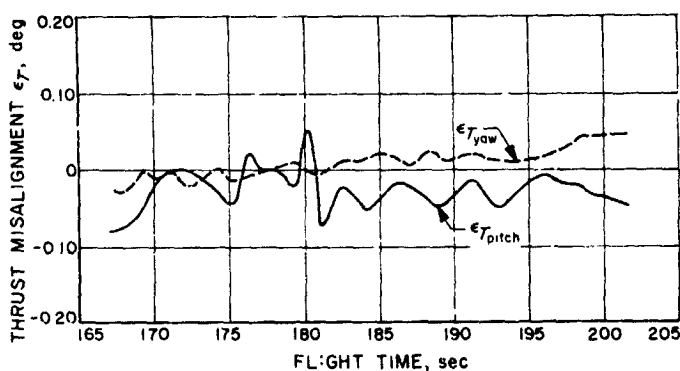

Fig. C-2. NASA Scout S-127 3rd stage pitch and yaw thrust misalignment vs time

component in the pitch direction and ζ_y being the component in the yaw direction. The maximum values do not necessarily occur simultaneously.

As seen in the table, the value for ζ rarely goes above 0.2 deg for stage 2 and stage 3. The weight of peroxide loaded on board for these two stages is based on a 0.25-deg thrust misalignment for the full duration of second stage burn, and 0.10-deg thrust misalignment for full duration for third stage burn. The peroxide supply has never been exhausted. Thus, from the above numbers, it is thought that a value of ζ of 0.004 rad (0.23 deg) is considered conservative for the examples considered in this Report.

Fig. C-1. NASA Scout S-127 2nd stage pitch and yaw thrust misalignment vs time

Table C-1. Scout thrust misalignment

Vehicle number	Second stage		Third stage	
	ζ_p max, deg	ζ_y max, deg	ζ_p max, deg	ζ_y max, deg
ST-6	0.100	0.074	0.026	0.011
ST-9	0.228	0.048	—	—
S-113	0.079	0.033	†	†
S-114	0.096	0.064	—	—
S-115	0.119	0.136	0.048	0.077
S-116	0.090	0.012	†	0.020
S-118	0.127	0.027	0.071	0.182
S-119	0.215	0.103	0.065	0.034
S-120	0.134	0.015	0.109†	0.455††
S-122	0.159	0.029	0.069	0.092
S-127	0.130	0.014	0.062	0.077
S-132	0.177	0.077	0.110	0.016

†Body oscillations obscured the "mean" rate data.
††Low thrust prior to burnout.

APPENDIX D

ZERO SPIN RATE

In certain applications, a short, high thrust with no spin may produce acceptable velocity dispersions (if the velocity increment is low enough). If such is the case, the small angle approximation made throughout Section IV no longer holds. Additionally, if the thrust misalignment is assumed constant (as it has been), the motion when $s_0 = 0$ is confined to two dimensions; either X_0 or Y_0 and Z_0. Referring to Fig. D-1, the curved path is the actual velocity path followed in the X_0-Z_0 plane, and the straight line (V) is the resultant velocity vector.

The angular acceleration of the body is a function of the torque, i.e.,

$$\ddot{\theta} = N = \frac{L}{I_x} = \frac{lF\zeta}{I_x} \tag{D-1}$$

whereupon, if the initial tip-off rate is $\dot{\theta}_0$,

$$\dot{\theta} = \dot{\theta}_0 + \frac{lF\zeta}{I_x} t, \text{ and integrating once again,}$$

$$\theta = \Theta_0 + \dot{\theta}_0 t + \frac{lF\zeta}{2I_x}t^2 \tag{D-2}$$

in Section III, $\Theta_0 = 0$ through the rotation of the inertial axes an angle Θ_0. The velocity components are then seen to be

$$V_x = \frac{gF}{m}\int_0^t \sin\theta \, dt$$

$$= \frac{gF}{m}\int_0^t \left(\sin\dot{\theta}_0 t \cos\frac{lF\zeta}{2I_x} t^2 + \cos\dot{\theta}_0 t \sin\frac{lF\zeta}{2I_x} t^2 \right) dt$$

and $V_z = \frac{gF}{m}\int_0^t \cos\theta \, dt$

$$= \frac{gF}{m}\int_0^t \left(\cos\dot{\theta}_0 t \cos\frac{lF\zeta}{2I_x} t^2 - \sin\dot{\theta}_0 t \sin\frac{lF\zeta}{2I_x} t^2 \right) dt \tag{D-3}$$
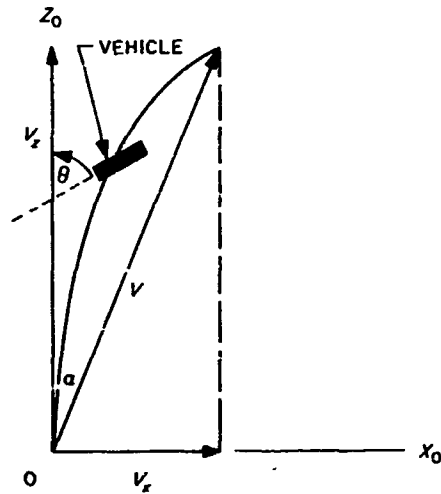

Fig. D-1. Velocity diagram when $S_0 = 0$

The integrals in Eq. (D-3) are seen to be modifications of the Fresnel integral, and if $\dot{\theta}_0 = 0$,

$$V_x = \left(\frac{\pi I_x g^2 F}{l\zeta m^2} \right)^{1/2} S\left\{ \sqrt{\frac{lF\zeta}{\pi I_x}} t \right\}$$

$$V_z = \left(\frac{\pi I_x g^2 F}{l\zeta m^2} \right)^{1/2} C\left\{ \sqrt{\frac{lF\zeta}{\pi I_x}} t \right\} \tag{D-4}$$

where C and S are defined in Section III-F. The error in the velocity direction is then

$$\alpha = \tan^{-1}\frac{V_x}{V_y} \tag{D-5}$$

and the error in the magnitude is $\left(1 - \frac{V_z}{V_z} \right)$.

Unless t_b is very small (< 1 second), V_x will probably be excessive. The velocity is necessarily kept small so that the thrust misalignment is reasonably bounded.

APPENDIX E

DESPINNING

After a body has been spun-up and a maneuver has occurred, it is often necessary to de-spin. The following is a brief listing of some despin devices:

1. Gas jet (hot or cold). The main drawback in addition to high weight is the fixed total impulse, which will despin only a fixed number of rpm. That is, if the jets work perfectly, a 10-rpm error in initial spin rate will also appear in the final spin rate.

2. Body-fixed magnetic rods in a magnetic field can also stop a rotating body (Ref. 13). However, this method has four main drawbacks: a magnetic field such as the Earth's) must be available, the time involved to stop the rotating body is considerable, all spin must be removed, and the use of magnetic rods in the body might have some interactions with other elements.

3. "Yo-yo's" are devices which decrease spin by releasing weights on cords which unwind due to the spin, causing large increases in inertia about the spin-axis. When the cords have unwound, they are released, taking with them the difference between the initial and final values of angular momentum.

Yo-yo's with both rigid and stretch cords have been investigated extensively in the past five years (Refs. 9, 14, 15, 16, 17). For reference, the necessary equations for the rigid cord yo-yo are given below, and are taken from Ref. 14. The deployment of a rigid cord yo-yo is depicted in Fig. E-1.

If ω_o = initial spin rate, rad/sec

$\dot{\theta}$ = final spin rate, rad/sec

γ = $\dot{\theta}/\omega_o$

m = mass of despin weight (for 1 cord), slug

I = inertia of spinning body about spin axis, slug-ft^2

a = radius of body (to cord attachment), ft

R = required length of cord, ft

T_{max} = maximum tension in cord, lb

t = time to despin, sec

then the length of one cord (there are 2 as shown in Fig. E-1) is

$$R = \left[\frac{(1-\gamma)(I+2ma^2)}{2m(1+\gamma)} \right]^{1/2} \qquad (E-1)$$

Note that this equation states that for a given R and m, $\gamma = \dot{\theta}/\omega_o$ is constant. Hence, yo-yo's take out a given
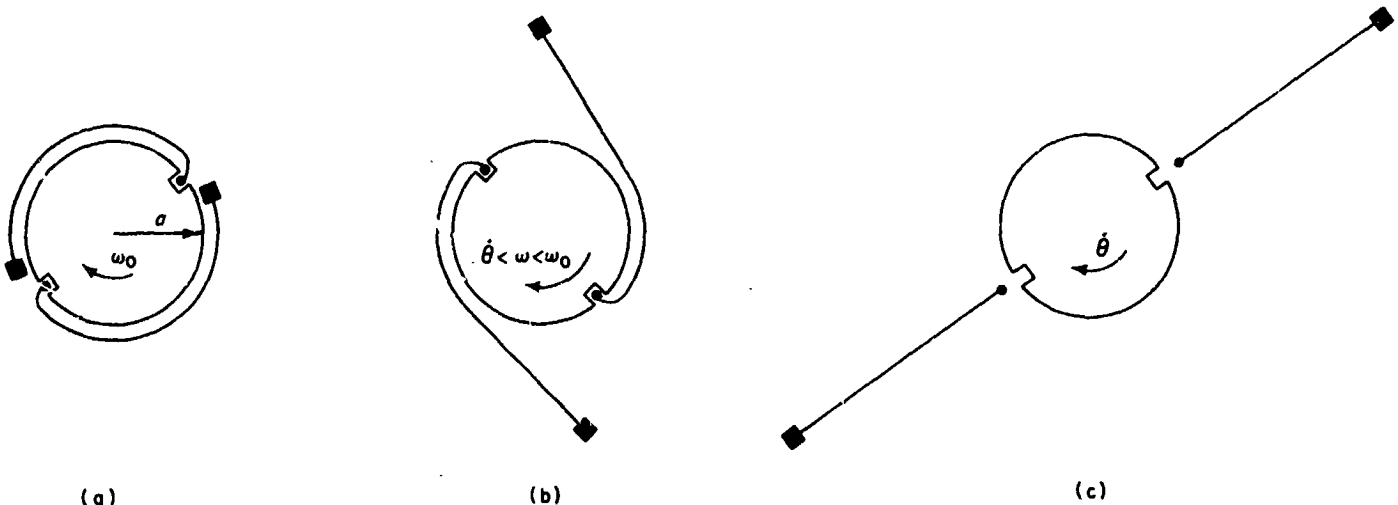

(a)   (b)   (c)

Fig. E-1. Rigid cord "yo-yo" deployment

proportion of spin, and a 1% error in initial spin rate will remain a 1% error after despin. However, if $\dot{\theta} = 0$, then Eq. (E-1) above becomes

$$R_0 = \left[\frac{I + 2ma^2}{2m} \right]^{\frac{1}{2}}$$

which states that to despin to 0 rpm, the dimensions of the despin mechanism (i.e., R_0 and m) are independent of ω_0. The time to despin is found by letting $R = a\omega_0 t$ in Eq. (E-1) and solving,

$$t = \frac{1}{a\omega_0} \left[\frac{(1-\gamma)(I+2ma^2)}{2m(1+\gamma)} \right]^{\frac{1}{2}}$$

Thus, the faster the body is spinning, the faster the yo-yo will stop it. The maximum tension in the cord (which is assumed massless) is

$$T_{max} = \frac{3I\omega_0^2}{4} \left[\frac{3m}{2(I+2ma^2)} \right]^{\frac{1}{2}}$$

When the stretch yo-yo is used, the effect of errors in the body inertia I, initial spin rate ω_0, cord length R and despin mass m is minimized.

ACKNOWLEDGMENT